DETERMINATION OF COMPLETE TEMPERATURE PROFILES OF SINGLY BURNING PULVERIZED FUEL PARTICLES

by

RONALD ALAN DICTOR

SUBMITTED IN PARTIAL FULFILLMENT
OF THE REQUIREMENTS FOR THE
DEGREES OF

BACHELOR OF SCIENCE IN CHEMICAL ENGINEERING

and

MASTER OF SCIENCE IN CHEMICAL ENGINEERING

at the

(August, 1979)

Signature of Author.....
Department of Chemical Engineering, August 31, 1979

Certified by.....
Thesis Supervisor

Accepted by.....
Chairman, Department Committee

DETERMINATION OF COMPLETE TEMPERATURE PROFILES OF SINGLY BURNING PULVERIZED FUEL PARTICLES

by

RONALD ALAN DICTOR

Submitted to the Department of Chemical Engineering

on August 31, 1979 in partial fulfillment of the requirements

for the Degrees of

Bachelor of Science in Chemical Engineering

and

Master of Science in Chemical Engineering

ABSTRACT

Experiments using two-color pyrometry were performed to determine the true temperature profiles of singly burning pulverized fuel particles. Montana lignite (as well as its char) was burned in a variety of oxidizing atmospheres above 1500 K to test for the effects oxygen partial pressure, particle size, gas temperature and volatile matter have on particle temperature and burnout time. Temperature profiles of particles burning in high oxygen concentrations were found to be erratic, but the average profiles consistently demonstrated a rise-fall behavior in temperature. The char profile did not clearly demonstrate the 'rise' which has since been attributed to the release and burning of volatile matter. At low oxygen partial pressures, particle temperatures monotonically increase during the course of a burnout. Particles burned hotter and slower in systems where argon was used as the diluent inert gas than in systems using helium. This is attributed to differences in diffusivity and thermal conductivity. The effects of particle size were qualitatively consistent with expectations, but no correlation was seen between particle size and burnout time. Lowering the gas temperature from 1791 K to 1536 K had a negligible effect on burnout times and temperature. Results were compared to an external diffusion-controlled combustion model which incorrectly predicted temperatures and burnout times. It appears that oxygen dissociation must be incorporated in any model of heat transfer.

Thesis Advisor: Adel F. Sarofim, Professor of Chemical Engineering

ACKNOWLEDGEMENTS

I approached Professor Adel Sarofim a while back seeking an interesting thesis topic, but instead he stuck me with a fascinating one. His own enthusiasm for this study was highly contagious, and I contracted a bad case of inspiration. For this and all his support I am much indebted and deeply grateful.

Special thanks go to Tony Modestino for all his support inside the lab as well as the patience he demonstrated while showing me the difference between a hammer and screwdriver. His interest and assistance made hard times bearable and good times enjoyable.

Thanks also to Chuck Mims, Don Coe, Ashwani Gupta and Brian Haynes for the guidance and helpful hints they provided. I wish to recognize and thank Richard Quann for his assistance in achieving single-particle flowrates that were necessary for this study. Matthew Neville's assistance in computer programming as well as his continuous feedback do not go unappreciated. I also thank him for limiting his singing while I was in the lab. My thanks also to all the other people, in the lab and outside, who helped make this study such an enjoyable experience.

Lastly, I give my heartfelt thanks to Debra Hickey - not for her drawings or for tailing me with a typewriter, but simply for making the whole endeavor so very worthwhile.

TABLE OF CONTENTS

Page

List of Figures

List of Tables

CHAPTER I

Introduction

The year 1979 is likely to be recorded in American history as a time of great change in energy policies. With the public aware that oil supplies are finite and nuclear accidents yet possible, increasing emphasis is being placed on coal utilization. Advances in technology have allowed us to gasify and liquefy coal, but for hundreds of years man has known that it may simply be burned.

Economic and environmental factors place major constraints on the direct utilization of coal in boilers. Ash deposits cause mechanical problems while soot, NO_x compounds and polycyclic aromatics pose potential threats to man's health. For these and other reasons, extensive research on coal combustion has been performed during the past 30 years. Amundson [1] provides a brief review of carbon combustion models and presents one of his own. In all of the models presented in the literature, the temperature of a burning carbon (or coal) particle is first estimated, and an overall heat balance is used to check the guess. There is a conspicuous dearth of single particle temperature data reported in the literature.

The goal of this study was to investigate, record and correlate the temperature histories of individual pulverized

fuel particles as they burned in various oxidizing atmospheres. Two-color pyrometry was the optical method used for temperature determination and is described in Chapter IV. Preliminary work was done at MIT in 1978 by Keith House and is documented in House's Bachelor thesis [7] and a report within the Department of Chemical Engineering. House developed a combustion model which is presented in Chapter III. Experimental data are compared to model predictions in Chapter V.

While reviewing this text the reader should bear in mind that coal combustion is a complex process. The quest for temperature data was made as an effort to answer many of the questions that have arisen in combustion modeling.

CHAPTER II

Background

The development of the two-color optical pyrometer is attributed to Hottel and Broughton [7]. They used the pyrometer to measure true temperature and total radiation of luminous flames. Much of the theoretical development they present is paralleled in Section 4.1.

In 1961 D. Rae [11] used the two-color method to determine the temperatures of frictional sparks. Rae noted that sensitivity of the system to changes in temperature is greatest when $(1/\lambda_B - 1/\lambda_A) = 2T/C2$, and he chose his photocells accordingly. λ_i are the effective wavelengths of the detectors, and C2 is a constant that will be defined later. Measurements were made in excess of $4000^{\circ}K$. Rae also used his intensity measurements to detect explosions of titanium particles.

In 1972 Ayling and Smith [2] burned pulverized fuel particles in a plug flow reactor that had several ports for optical access. They used a single photomultiplier with rotating filters to view the stream of particles passing by a single port. The temperatures they measured were fitted to a heat balance and it was determined that carbon monoxide was the primary product at the particle surface. The authors also noted that temperatures fell with decreasing

particle size in 20 percent oxygen.

Ubhayakar and Williams [13] were the first to apply the two-color pyrometry method to singly burning particles. They suspended electrode carbon particles in oil droplets on the end of a thread and ignited them with a laser. Particles burned in gases held at ambient temperature. Use of high speed cinemicrography enabled them to conclude that the reaction zone was restricted to the particle surface and the square of the particle diameter decreased linearly with time. The data were fitted to an Arrhenius expression consistent with carbon monoxide formation. Many of the experimentally determined temperatures were several hundred degrees above model predictions. Temperatures above 4000 K were not uncommon for particles burning in 100 percent oxygen.

In 1978 Keith House [8] began temperature studies at MIT. House viewed particles as they flowed past a water-cooled optics probe that was inserted up the bottom of a quartz laminar-flow furnace. Light was split and guided to two infra-red detectors. The signals from the detectors were amplified and displayed on an oscilloscope.

This study is an extension of House's work. Modifications to his system were made so that complete (ignition → extinction) temperature profiles could be determined. A non-invasive technique was sought to gather light from the fuel particle; the gas temperature profile in House's

furnace was uncharacterized because of the presence of a water-cooled probe.

CHAPTER III

A Diffusion-Controlled Coal Combustion Model

In the summer of 1978, House proposed a diffusion-controlled coal combustion model in a report submitted within the Department of Chemical Engineering at MIT. As part of this study, a comparison was made between model-predicted temperature profiles and burnout times and those obtained experimentally.

3.1 The Model

Few changes were made in House's model as it is reproduced here. Those that were made will be noted during the derivation. We start with the beginning assumptions:

i) Volatiles are instantaneously released and burned. The residual char is modeled as a shrinking, burning carbon sphere with a density of the char residue.

ii) Pseudo steady-state heat and mass transfer are rapidly attained.

iii) The combustion rate is mass transfer limited.

iv) The primary reaction $2C + O_2 \rightarrow 2CO$ occurs on the surface of the particle.

v) The oxidation of CO to CO_2 occurs far enough away from the particle surface that it has little or

no influence on particle temperature.

vi) The two modes of heat transfer are conduction and radiation; convection is negligible.

vii) The emissivity of the particle is unity.

viii) The effects of oxygen dissociation in the boundary layer are negligible.

ix) Ash does not influence the combustion rate.

A steady-state heat balance about a burning particle gives:

$$-k \frac{dT}{dr} = \frac{R \cdot (-\Delta H_{rxn})_T - Q}{4\pi r^2} \tag{3.1}$$

where k is the gas thermal conductivity, $(-\Delta H_{rxn})_T$ is the heat of reaction at temperature T, R is the reaction rate in gram-moles O_2/sec. and Q is the radiative heat loss term.

$$Q = 4\pi r_p^2 \sigma (T_p^4 - T_w^4) \tag{3.2}$$

Here σ is the Stefan-Boltzmann constant, and the subscripts p and w refer to the particle surface and furnace walls, respectively. Using data from the literature, House approximated thermal conductivity and heat of reaction as linear functions of temperature:

$$k = C_k \cdot T \tag{3.3}$$

$$(-\Delta H_{rxn})_T = C_{H1} + C_{H2} \cdot T \tag{3.4}$$

Equation (3.3) provides an excellent approximation for thermal conductivity at low gas temperatures, but at temperatures in excess of 1800 K.

$$k = C_{K1} + C_{K2} \cdot T \tag{3.5}$$

yields more accurate values. Combining equations (3.4) and (3.5) with equation (3.1) and using the boundary conditions

$$T = T_p \text{ at } r = r_p$$

$$T = T_\infty \text{ at } r = \infty \tag{3.6}$$

one may integrate and find this closed-form solution for R:

$$R = \frac{4\pi r_p}{C_{H2}} \left[\left(C_{K1} + \frac{C_{K2}}{C_{H2}} (Q/R - C_{H1}) \right) \ln \left(\frac{C_{H1} + C_{H2} T_p - Q/R}{C_{H1} + C_{H2} T_\infty - Q/R} \right) + C_{K2} (T_p - T_\infty) \right] \tag{3.7}$$

Equation (3.7) is an expression for the reaction rate based solely on a heat balance. For a diffusion-controlled model, this expression for R must equal the rate at which O_2 arrives at the particle surface. From assumption (*ii*) we know that

$$-4\pi r^2 N_{O_2} = \text{constant} = R \tag{3.8}$$

where N_{O_2} is the radial flux of oxygen.

Since the primary reaction is the formation of carbon monoxide, the flux of CO will be twice that of O_2 in the

opposite direction:

$$-2N_{O_2} = N_{CO} \tag{3.9}$$

Fick's Law states that

$$N_{O_2} = -cD \frac{dX_{O_2}}{dr} + X_{O_2}(N_{O_2} + N_{CO}) \tag{3.10}$$

Combining equations (3.8), (3.9) and (3.10):

$$\frac{dX_{O_2}}{1+X_{O_2}} = \frac{R}{4\pi cD} \frac{dr}{r^2} \tag{3.11}$$

The diffusivity term is also approximated as a linear function of temperature:

$$cD = C_{D1} + C_{D2} \cdot T \tag{3.12}$$

With this approximation equation (3.11) may be solved by integrating from the particle surface to the bulk gas:

$$\ln(1+X_{O_{2\infty}}) = \sum_{r_p}^{\infty} \frac{\Delta r}{r^2} (C_{D1} + C_{D2} \cdot T)^{-1} \frac{R}{4\pi} \tag{3.13}$$

$X_{O_{2\infty}}$ is the bulk mole fraction of oxygen, and $X_{O_2} = 0$ at the particle surface.

Equation (3.13) may be given a closed-form solution if a simple temperature functionality is substituted for $\Delta r/r^2$. If we return to equation (3.1) and neglect the temperature dependence of the heat of reaction, one can show that

$$\frac{r}{r_p} = \frac{C_{K1}(T_\infty - T_p) + \frac{C_{K2}}{2}(T_\infty^2 - T_p^2)}{C_{K1}(T_\infty - T) + \frac{C_{K2}}{2}(T_\infty^2 - T^2)} \quad . \tag{3.14}$$

Substituting this expression into equation (3.13) and integrating one finds that

$$\ln(1+X_{O_{2\infty}}) = \frac{aRC_{K2}}{4\pi C_{D2}} \left[\left(\frac{C_{K1}}{C_{K2}} - \frac{C_{D1}}{C_{D2}} \right) \ln \left[\frac{C_{D1} + C_{D2}T_\infty}{C_{D1} + C_{D2}T_p} \right] + T_\infty - T_P \right]$$

$$\frac{1}{a} = r_p \left[C_{K1}(T_\infty - T_p) + \frac{C_{K2}}{2}(T_\infty^2 - T_p^2) \right] \tag{3.15}$$

Given the appropriate physical parameters along with particle radius, bulk temperature and bulk oxygen concentration, equations (3.7) and (3.15) can be used to deduce both the rate of chemical reaction and the particle temperature.

3.2 Burnout Times

Burnout times were calculated simply on the basis of a shrinking core model. Ignition occurs when the radius of the burning particle is at its initial value, and extinction occurs when the radius equals zero. The burnout time is the time between ignition and extinction. If S grams of carbon are consumed per mole of O_2 reacted, then $S \cdot R$ grams are consumed per second and

$$S \cdot R \cdot \Delta t = \rho 4\pi r_p^2 \Delta r_p \tag{3.16}$$

where the right-hand side is the shell of carbon consumed from the sphere in time Δt. ρ is the density of the particle. Since temperature is a weak function of particle size and radiative heat loss is small compared to conductive loss, one can say using equation (3.7) that

$$\frac{R}{r_p} \approx \text{constant} \approx \left(\frac{R}{r_p}\right)_0 \tag{3.17}$$

Substituting into equation (3.16) and rearranging:

$$\Delta t = \left(\frac{r_p}{R}\right)_0 \cdot \frac{4\pi\rho}{S} \cdot r_p \Delta r_p \tag{3.18}$$

This equation may be integrated from ignition to extinction to give the burnout time:

$$t_{b.o.} = \left(\frac{r_p}{R}\right)_0 \frac{2\pi\rho}{S} (r_p)_0^2 \tag{3.19}$$

The value of R/r_p is not truly constant, and House corrects for this by using the value at the time-averaged radius:

$$r_{avg} = \frac{\int r dt}{t_{b.o.}} = \frac{2}{3}(r_p)_0 \tag{3.20}$$

The above result is reached by substituting equation (3.18) in the integral and dividing by equation (3.19). The final result is

$$t_{b.o.} = \left[\left(\frac{r_p}{R}\right)_{r_p=2/3(r_p)_0}\right] \frac{2\pi\rho}{S} (r_p)_0^2 \qquad (3.21)$$

R is derived from equations (3.7) and (3.15), S = 24 g/g-mole for the carbon monoxide reaction, and ρ is approximately 0.5 g/cc for char produced from Montana Lignite.

3.3 Examining the Model

The predictions given by the model are qualified by the assumptions referred to earlier. The model neglects devolitilization, ash vaporization, impurities, pore structure, surface phenomena and water reactions. The list of simplifications is far from complete. Still the model may be useful in providing some limited insight into the burning characteristics of coal.

A computer program was written using equations (3.7), (3.15) and (3.21); it has been reproduced in Appendix C. The program calculates the temperature of a burning carbon sphere as functions of both real time and dimensionless time. The dimensionless time is simply time into burnout divided by total burnout time (0 for ignition and 1 for extinction). Figures 3.1 - 3.4 were produced to illustrate the influence some of the model parameters have on particle temperature.

Figure 3.1 shows the increase in particle temperature with increasing oxygen partial pressure in an O_2-Ar system; the rate of the temperature increase is greatest at low

Figure 3.1 .Effect of Oxygen Partial Pressure on Particle Temperature

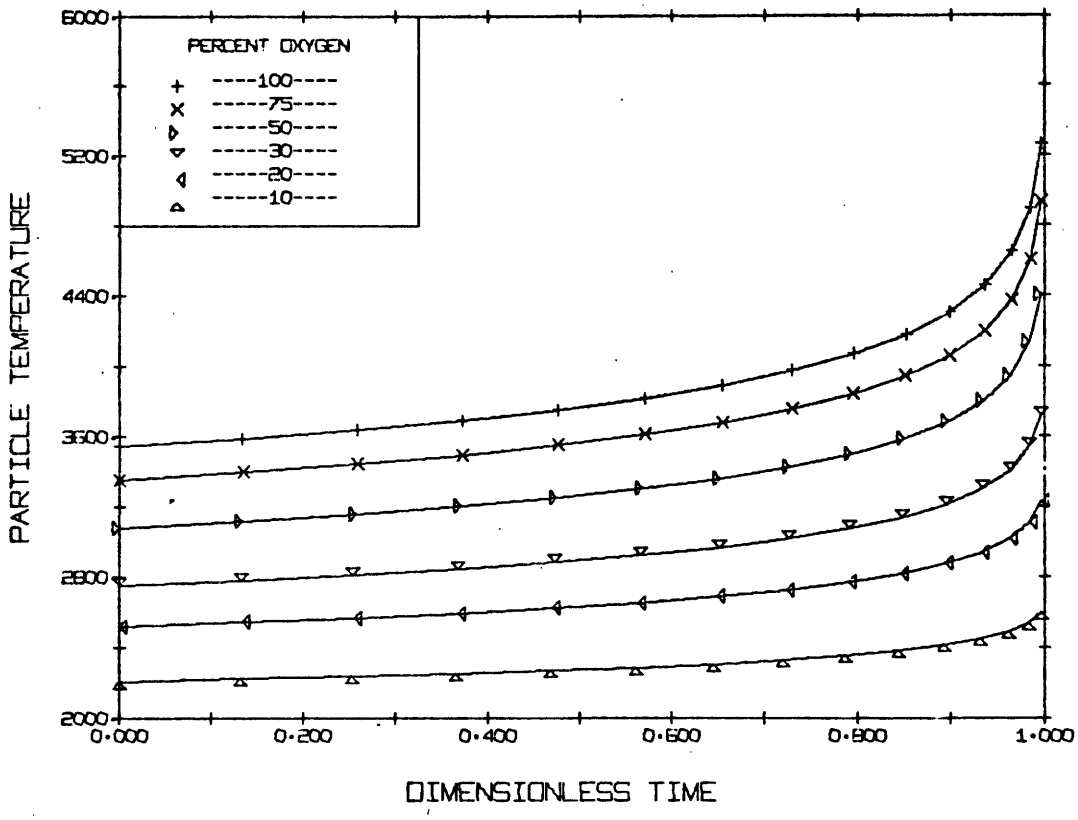

Figure 3.2 Effects of Particle Size on Temperature

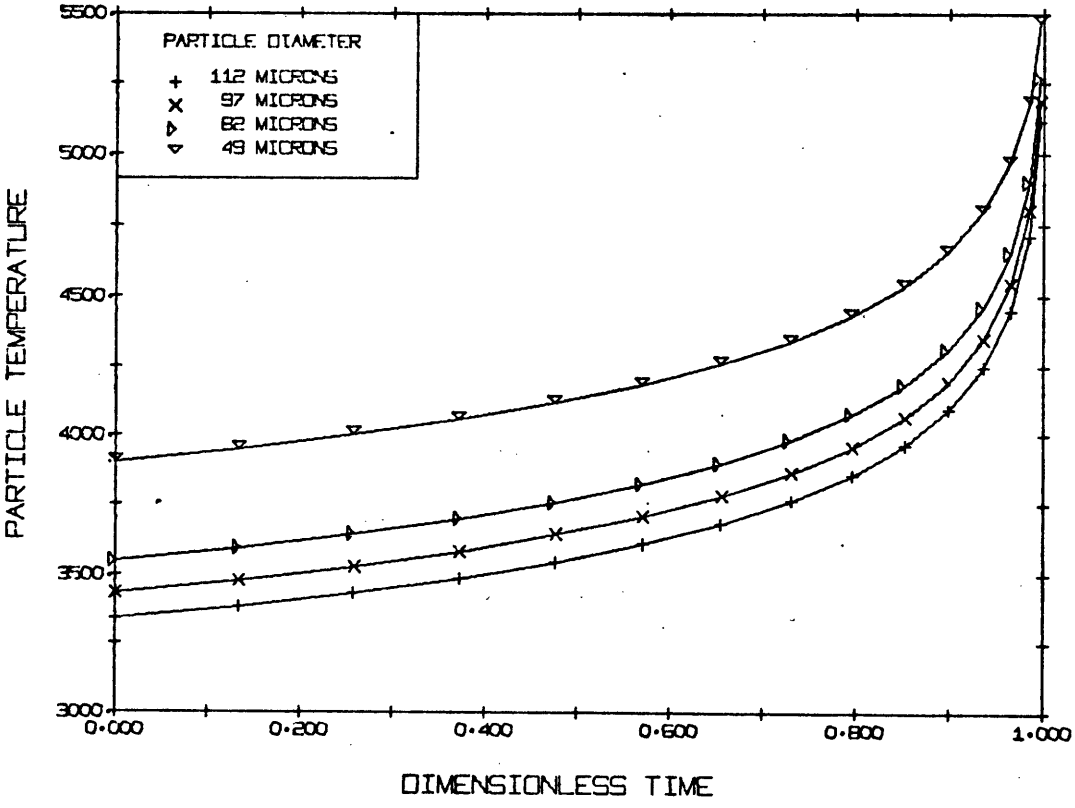

Figure 3.3 Particle Temperature at Different Gas and Well Temperatures

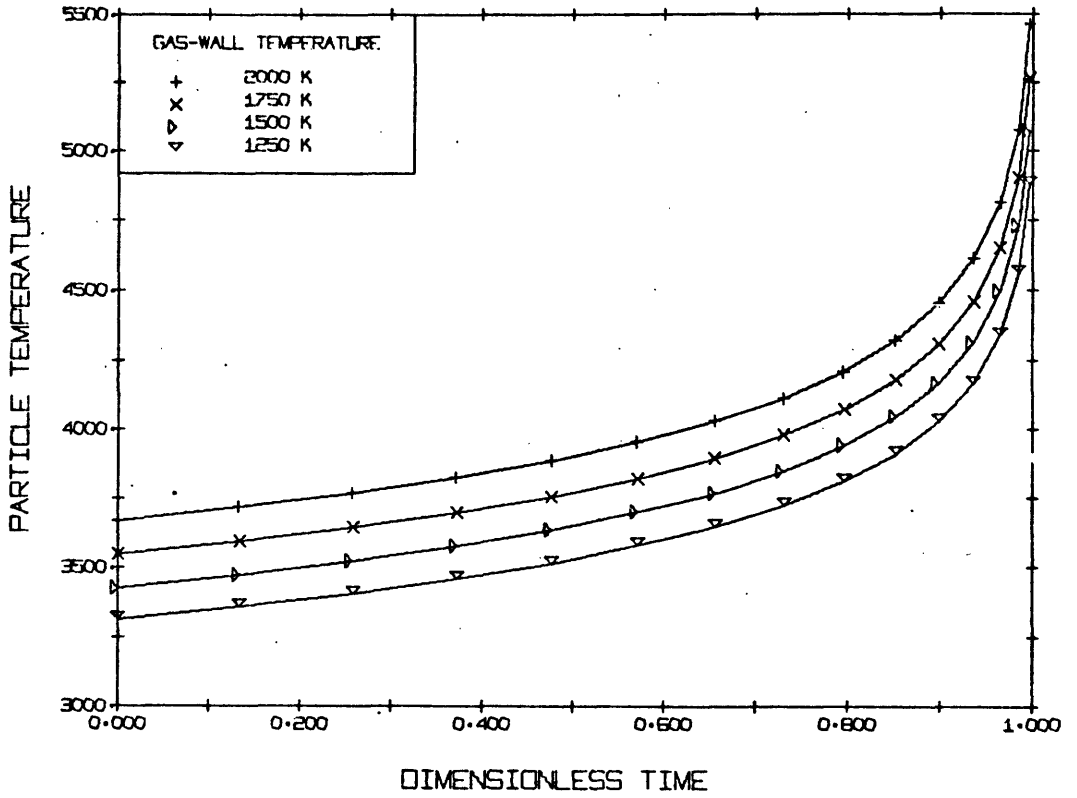

Figure 3.4 Influence of Heat of Reaction on Particle Temperature

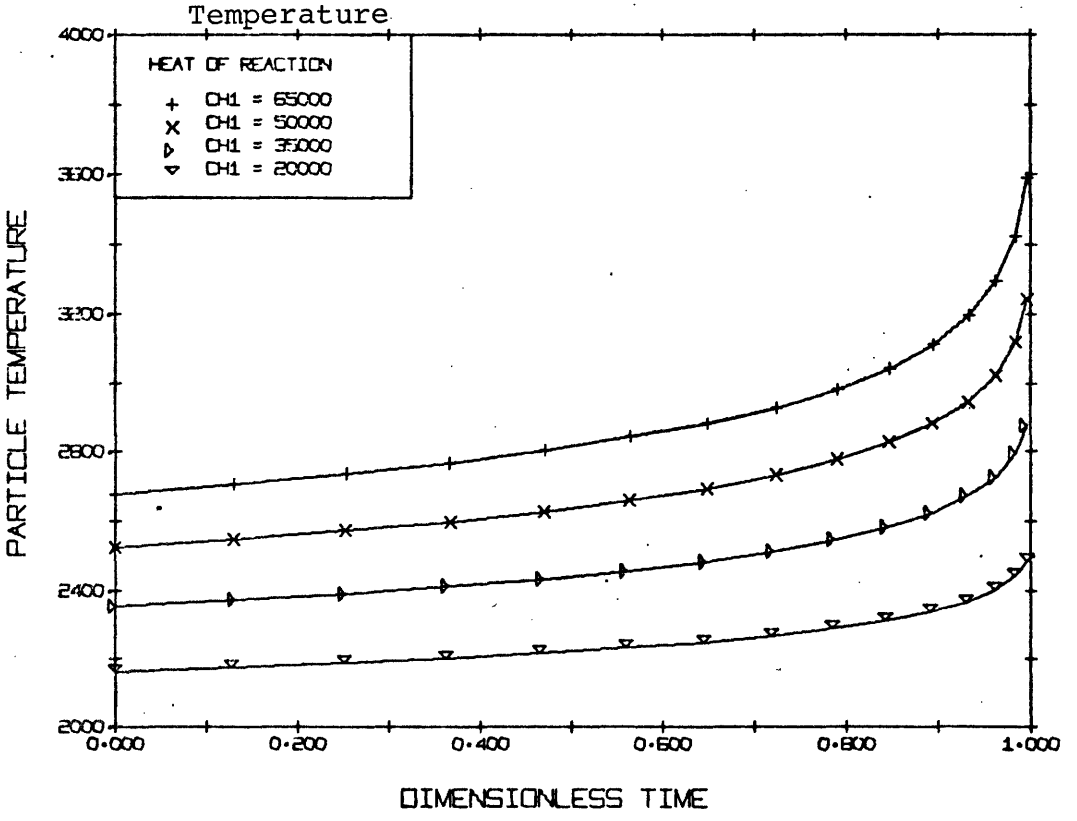

partial pressures. The temperature of a particle rises near the very end of a burnout as a consequence of the decrease in importance of radiation relative to conduction as the particle size decreases.

Because particle temperatures increase with burnout and the transport mechanisms are at (pseudo) steady-state, temperature must rise with decreasing particle size. This is illustrated in Fig. 3.2 which shows four different sized particles burning in 100 percent oxygen at 1750 K.

Figure 3.3 shows particle temperature as a function of gas and wall temperatures for particles burning in 100 percent oxygen. Figure 3.4 demonstrates the sensitivity of temperature to heat of reaction in a system of 20 percent oxygen in argon. As discussed earlier, Ayling and Smith [2] used the heat of reaction to predict particle temperature and deduce that carbon monoxide is the primary combustion product.

Before continuing it should be noted that several of the foregoing 'tests' were performed using parameters consistent with a helium-oxygen system. Iterations to find reaction rates and temperatures in systems with high oxygen partial pressures would not converge because of the mismatching of diffusivity and thermal conductivity constants. The model does not take into account the physical properties of the combustion products. The model predictions are likely to be more consistent with Ar - O_2 data than with He - O_2

data because argon's physical properties more closely resemble those of both carbon monoxide and oxygen.

CHAPTER IV

Experimental Design

The task of obtaining temperature-time profiles of singly burning fuel particles is not a simple one. Temperatures might exceed 3000 K, the total duration of the burnout may be a few milliseconds, and particle sizes are on the order of microns. The nature of this project precluded the use of any non-optical means for measuring surface temperatures.

4.1 Two-Color Pyrometry

The light intensity of a burning coal particle at any wavelength λ is proportional to the particle's surface area and a strong function of temperature and emissivity. The latter is given by Planck's Law [3]:

$$q_\lambda = \frac{2\pi c^2 h \epsilon_\lambda}{\lambda^5} \left(\exp\left[\frac{ch}{2KT}\right] - 1 \right)^{-1} \qquad (4.1)$$

where c is the speed of light, h is Planck's constant, K is Boltzmann's constant, T is the particle temperature, λ is the wavelength and ϵ_λ the emissivity at that wavelength. The emissivity is itself a function of temperature. $2\pi c^2 h$ is Planck's first radiation constant, C1, and equals 3.74 x 10^{-12} watts $\cdot$ cm^2. Similarly, ch/K is Planck's second

radiation constant, C2, and equals 1.44 cm · K. For exp (C2/λT) >> 1 we can use Wien's approximation and disregard the unity term on the right-hand side of equation (4.1). The radiative flux at λ is now given by:

$$q_\lambda = \frac{\epsilon_\lambda C1}{\lambda^5} \exp\left[\frac{-C2}{\lambda T}\right] \tag{4.2}$$

Particle temperature cannot be directly determined using equation (4.2): the emissivity is unknown.

In two-color pyrometry one is concerned not with absolute intensity at one wavelength but rather with the ratio of two intensities from two different wavelengths, λ_A and λ_B. Assuming that emissivity is not a function of wavelength (grey body), the ratio ϵ_A/ϵ_B becomes unity and we have

$$\frac{\int_{\lambda_A - \frac{\Delta\lambda_A}{2}}^{\lambda_A + \frac{\Delta\lambda_A}{2}} q_{\lambda A} d\lambda}{\int_{\lambda_B - \frac{\Delta\lambda_B}{2}}^{\lambda_B + \frac{\Delta\lambda_B}{2}} q_{\lambda B} d\lambda} = f(T,\lambda) \tag{4.3}$$

The measured intensity at each wavelength will depend on system parameters such as the amount of light carried to the detectors and the detector efficiency. The latter is often very dependent on wavelength. If the bandwidths of

interest are sufficiently narrow we can assume the average efficiency of the detector within a bandwidth to be that of the peak wavelength. We can approximate equation (4.3) by

$$\frac{I_A}{I_B} = \frac{\eta_{L,A}\eta_{D,A}\lambda_B^5 \exp\left(\frac{-C2}{\lambda_A T}\right)\Delta\lambda_A}{\eta_{L,B}\eta_{D,B}\lambda_A^5 \exp\left(\frac{-C2}{\lambda_B T}\right)\Delta\lambda_B}$$

$$= \frac{\eta_{L,A}\eta_{D,A}\lambda_B^5\Delta\lambda_A}{\eta_{L,B}\eta_{D,B}\lambda_A^5\Delta\lambda_B} \exp\left[\frac{C2}{T}\left(\frac{1}{\lambda_B} - \frac{1}{\lambda_A}\right)\right] \qquad (4.4)$$

Where I_i are the measured intensities, $\Delta\lambda_i$ are the bandwidths used in the detection, $\eta_{L,i}$ are the efficiencies for carrying light to the detectors and $\eta_{D,i}$ are the detector efficiencies at each wavelength. The ratio of emissivities is assumed to equal unity. All of the coefficients for the exponential term in the above equation can be combined into one calibration constant leaving us with

$$\frac{I_A}{I_B} = C \exp\left[\frac{C2}{T}\left(\frac{1}{\lambda_A} - \frac{1}{\lambda_B}\right)\right] \qquad (4.5)$$

or

$$T = \frac{C2\left(\frac{1}{\lambda_A} - \frac{1}{\lambda_B}\right)}{\ln\frac{I_A}{I_B} - \ln C} \qquad (4.6)$$

where $C = \dfrac{\eta_{L,A}\eta_{D,A}\lambda_B^5\Delta\lambda_A}{\eta_{L,B}\eta_{D,B}\lambda_A^5\Delta\lambda_B}$.

This approximation is good only for narrow bandwidths. (See Appendix B.)

4.2 Optical Access to the Burning Particle

Temperature studies were done using the Astro (model #1000 A) laminar flow furnace illustrated in Figure 4.1. Particles were entrained in a carrier gas and fed to the combustion zone through a water-cooled probe. The oxidizing gas enters this zone through a honeycomb which is used to straighten the gas flow as well as heat the gas. The viewing port in the wall of the furnace could not be used because of the alumina muffle tube.

The only options available for gaining optical access to the furnace were to look at the combustion zone from above or below. Because a cold background is necessary for viewing the particles, any set-up at the bottom of the furnace would have required that we focus on the tip of the feeder probe and block out all the light from the walls and honeycomb. On the other hand, access from the top meant viewing and feeding through the feeder probe simultaneously. This appeared to be the better of the two options.

Figure 4.2 is a schematic of the optical system used. Alongside each component is an upper estimate of the loss factor, i.e. fraction of light transmitted. The greatest loss factor is obviously in the feeder tube itself. The tube has an inside diameter of .160" and a length of 19".

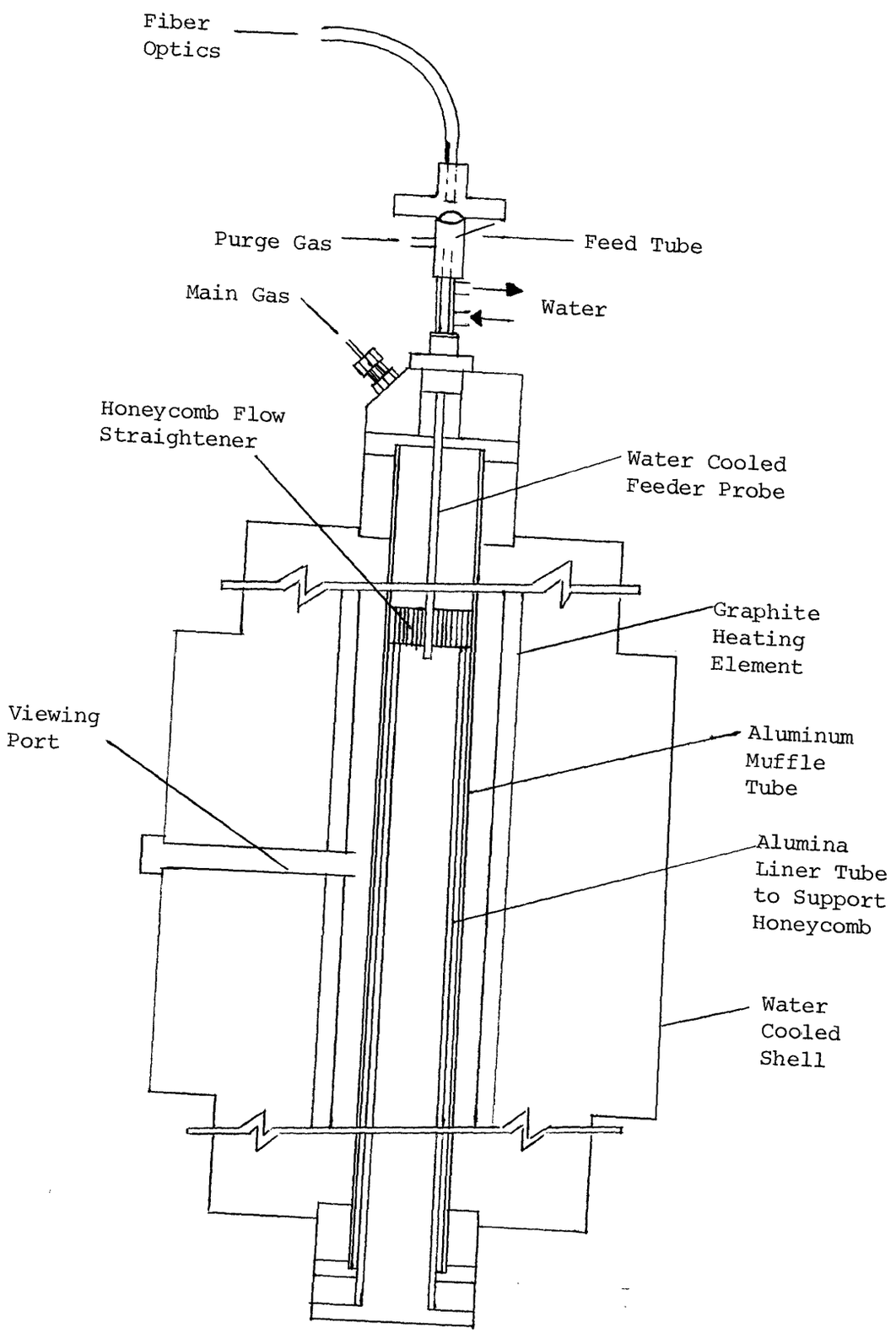

Figure 4.1: Laminar Flow Furnace

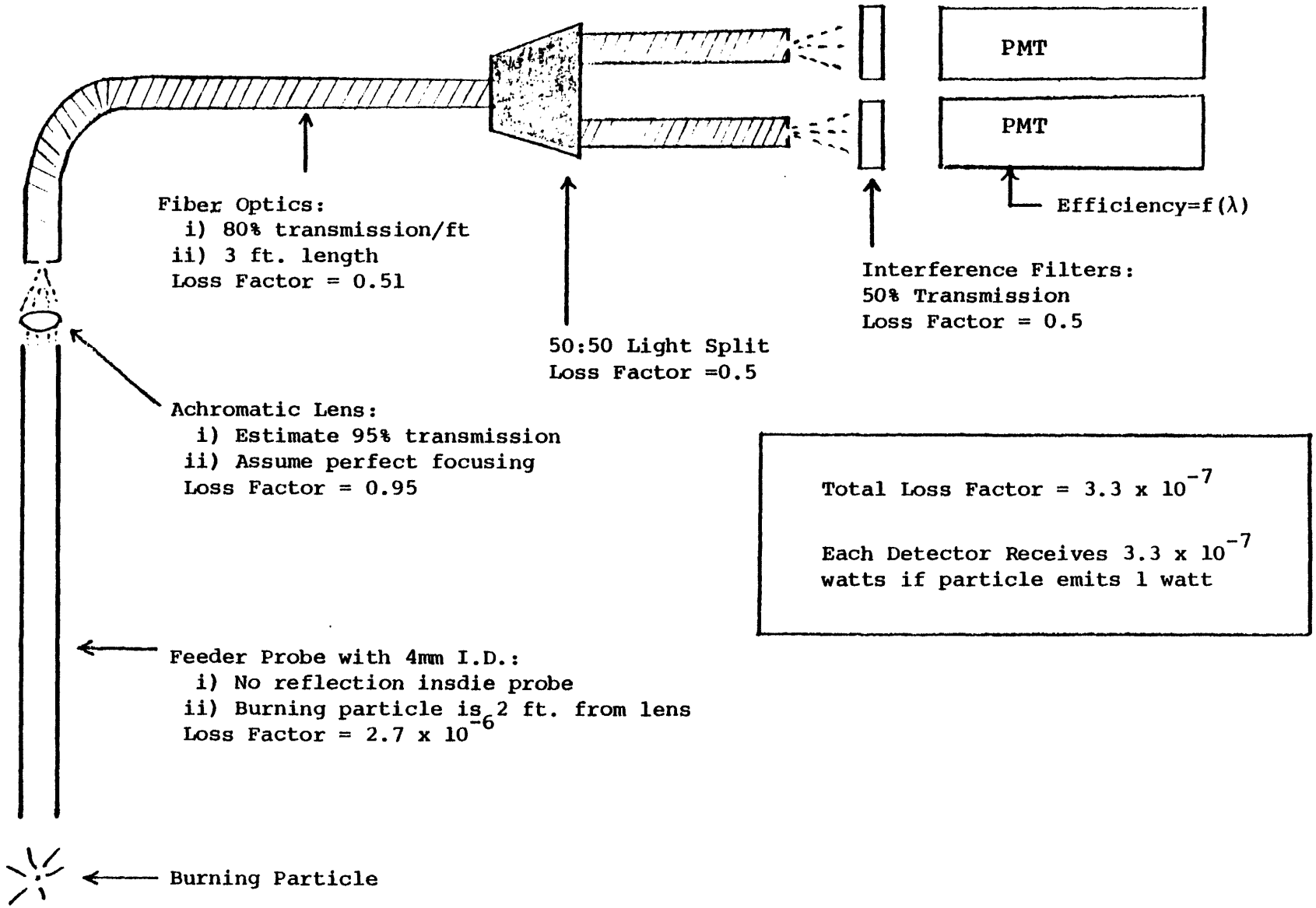

Figure 4.2: Analysis of the Optical System

Calculations of the system's geometry showed that only the bottom 2 1/2" - 3" of the feeder probe needed to be blackened to prevent radiation from the furnace walls from reaching the detectors. Flat black paint was sprayed freely inside the tube, but some background light was still seen because of the paint's non-zero reflectivity.

4.3 Choice of Detectors

House's work with the probe enabled him to use silicon infra-red detectors with single-stage current amplifiers. His work was done in the near infra-red region (.75 μm and .94 μm) because of the sensitivity of the ratio of two intensities to small changes in temperature. The same detectors were originally used in this study, but the geometry of the set-up necessitated a move to more sensitive detectors.

Two EMI - GENCOM model # 9824B photomultiplier tubes (PMT's) were magnetically shielded and mounted above the furnace in light-proof housings. Each of the 11-stage PMT's had a standard dynode chain totalling 1.4 Megohms. The overall voltage applied to the tubes was typically 650 to 750 volts. At 450 nanometers the bialkali photocathode material has an absolute sensitivity of 84 milliamperes per watt, and at 550 nanometers this value is 37 milliamperes per watt. With a 700 V applied voltage, the PMT's have a gain of 3×10^5. All of these figures are reproduced from the manufacturer's literature. The dark current of each PMT

was tested and found to be below 2 nanoamps, so it was assumed that the PMT's were in good working condition.

A round, one-inch interference filter was placed in each PMT housing between the fiber optics cable and the photocathode. The filter defined as 'A' transmitted light at 450 nm, and that defined as 'B' transmitted at 550 nm. Each filter had roughly a 4 - nanometer bandwidth. Calculations using an integrated form of equation (4.2) showed a loss of intensity of no more than two orders of magnitude when dropping down Planck's radiation curve at 1600 K (Appendix B) from House's near infra-red region to the visible region. The gain of PMT exceeds that of the IR detector by four orders of magnitude, so the net result is approximately a 100-fold improvement in sensitivity at that temperature.

The anode currents were continuously dropped across 1MΩ resistors, and the voltages were measured on a Tektronix T912 storage oscilloscope. The 1MΩ impedance of the scope in parallel with the 1MΩ resistor yielded an effective resistance of 0.5 MΩ. No amplification was required for the combustion conditions reported here.

4.4 Single Particle Feed System

The importance of reducing the feed rate to single-particle flow cannot be overemphasized. Unpublished vaporization studies performed on the same furnace indicate that

increasing feed rate enhances vaporization, presumably because of longer burning times due to localized depletion of oxygen. Capturing the two-color traces of a single particle in a field of several particles is not possible with the system described above. While single-particle flow is important for modeling purposes, one must be aware that information on combustion products and vaporization is being sacrificed.

The author wishes to credit Richard Quann and Charles Mims for the 2-stage feed system depicted in Figure 4.3. The first stage (on the right) consists of a vial of coal mounted in a vacuum seal on a syringe pump. The vial is slowly pushed upward as an inert carrier gas sweeps coal out of the vial and into the 20-gauge needle. The coal emerges from the bottom tube in the dilution chamber in the form of a steady stream. By adjusting the collection tube above the stream, the particle flow can be diluted until single-particle flow is obtained.

Particles flow from the dilution chamber to the furnace in a thin Tygon tube and enter at the bottom of the optics mount below the lens. A light purge gas enters the mount just above this stream to prevent build-up of particulates on the lens. The mount itself, shown in Figures 4.1 and 4.3, is comprised of two pieces that allow for easy focusing of light onto the fiber optics surface. Particles flow freely in the carrier gas from the entrance in the mount to the

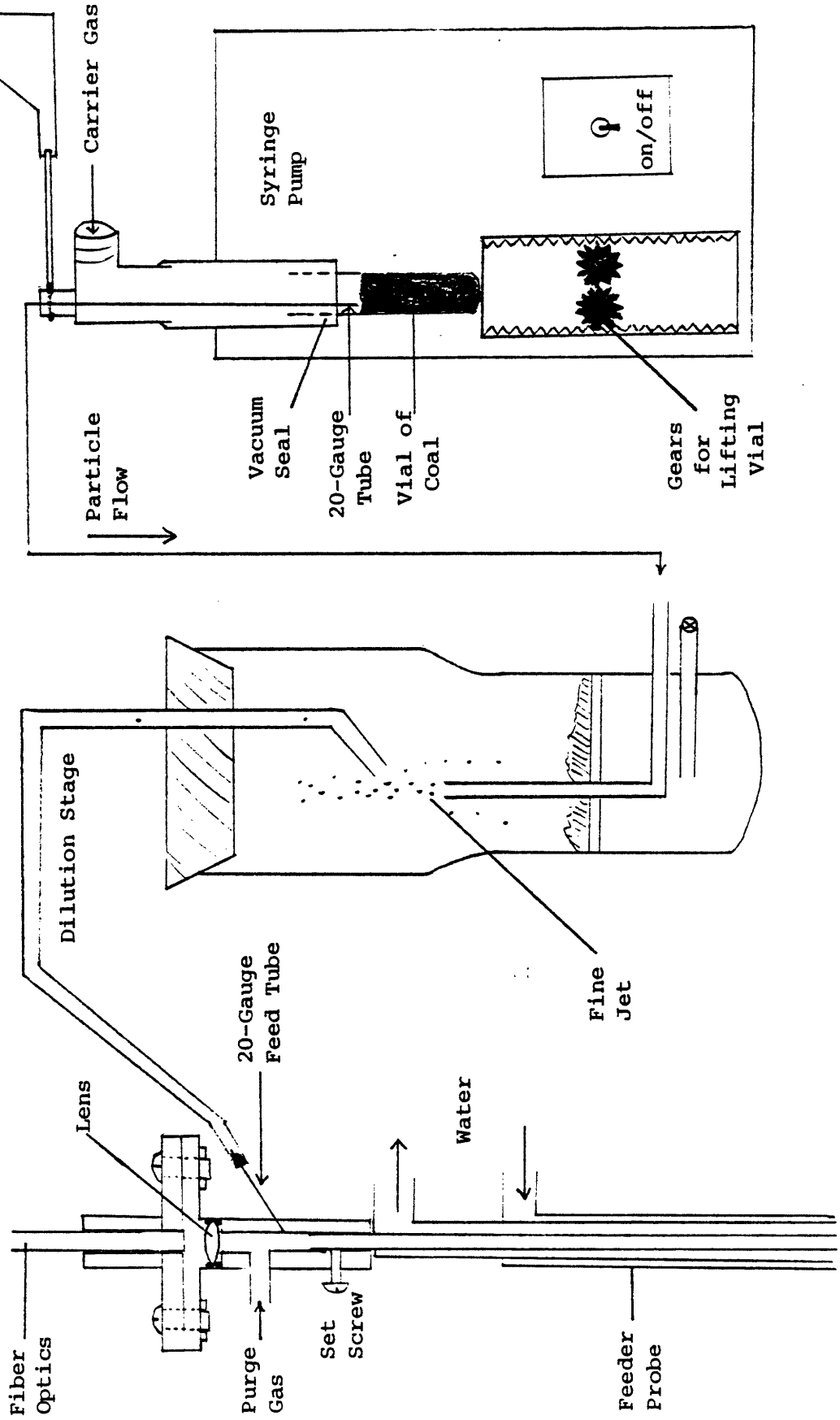

Figure 4.3: Two-Stage Single Particle Feed System

combustion zone within the furnace.

4.5 Calibrations

The calibration constant seen in equation (4.5) must be experimentally determined at the time of each temperature study. Photomultiplier tubes display a 'drift' with time; frequent calibrations are needed.

A General Electric tungsten strip lamp was mounted directly beneath the furnace such that the strip was optically aligned with the feeder probe. A Hewlett-Packard (model #6268B) regulated power supply was randomly adjusted to provide different lamp temperatures. Brightness temperatures were measured with a Pyro Micro-Optical Pyrometer (Pyrometer Instrument Co.) disappearing filament pyrometer, and corresponding voltages from the PMT's were measured on a digital voltmeter.

The brightness temperature (T_b) of tungsten was converted to true temperature (T_t) by use of the definition

$$\frac{C1}{\lambda^5}\left(\exp\left[\frac{C2}{\lambda T_b}\right]-1\right)^{-1} = \frac{\epsilon_\lambda C1}{\lambda^5}\left(\exp\left[\frac{C2}{\lambda T_T}\right]-1\right)^{-1} \qquad (4.7)$$

Rearranging and using Wein's approximation:

$$T_t = \left(\frac{\lambda}{C2}\ln\epsilon_\lambda + \frac{1}{T_b}\right)^{-1} \qquad (4.8)$$

Rutgers and De Vos [12] provide an excellent nomogram that relates brightness temperature to true temperature for a

tungsten strip at 650 nm, the effective wavelength of the pyrometer.

The calibration constant is easily derived from equation (4.5) (with emissivities included):

$$\ln C = \ln \frac{I_A}{I_B} - \ln \frac{\epsilon_A}{\epsilon_B} + \frac{C2}{T_t} \left(\frac{1}{\lambda_A} - \frac{1}{\lambda_B} \right) \qquad (4.9)$$

De Vos [5] supplies emissivity data for tungsten.

4.6 Operational Procedure

The operating procedure initially adhered to is as follows:

i) Take 6 to 10 calibration points including background (tungsten lamp turned off)

ii) Set gas controls to desired values. Gas flowrate was always 6 l/min. except in cases of 100 percent oxygen (5 l/min.).

iii) Begin feeding coal. Adjust flowrate until individual traces could easily be obtained on the storage oscilloscope.

iv) Photograph several 'burnout peaks' using the Polaroid camera attachment for the oscilloscope.

v) Capture approximately 100 traces on the oscilloscope for purposes of measuring only the burnout times. Record.

vi) Calibrate and repeat starting at *ii*.

The schedule was not strictly followed as it was

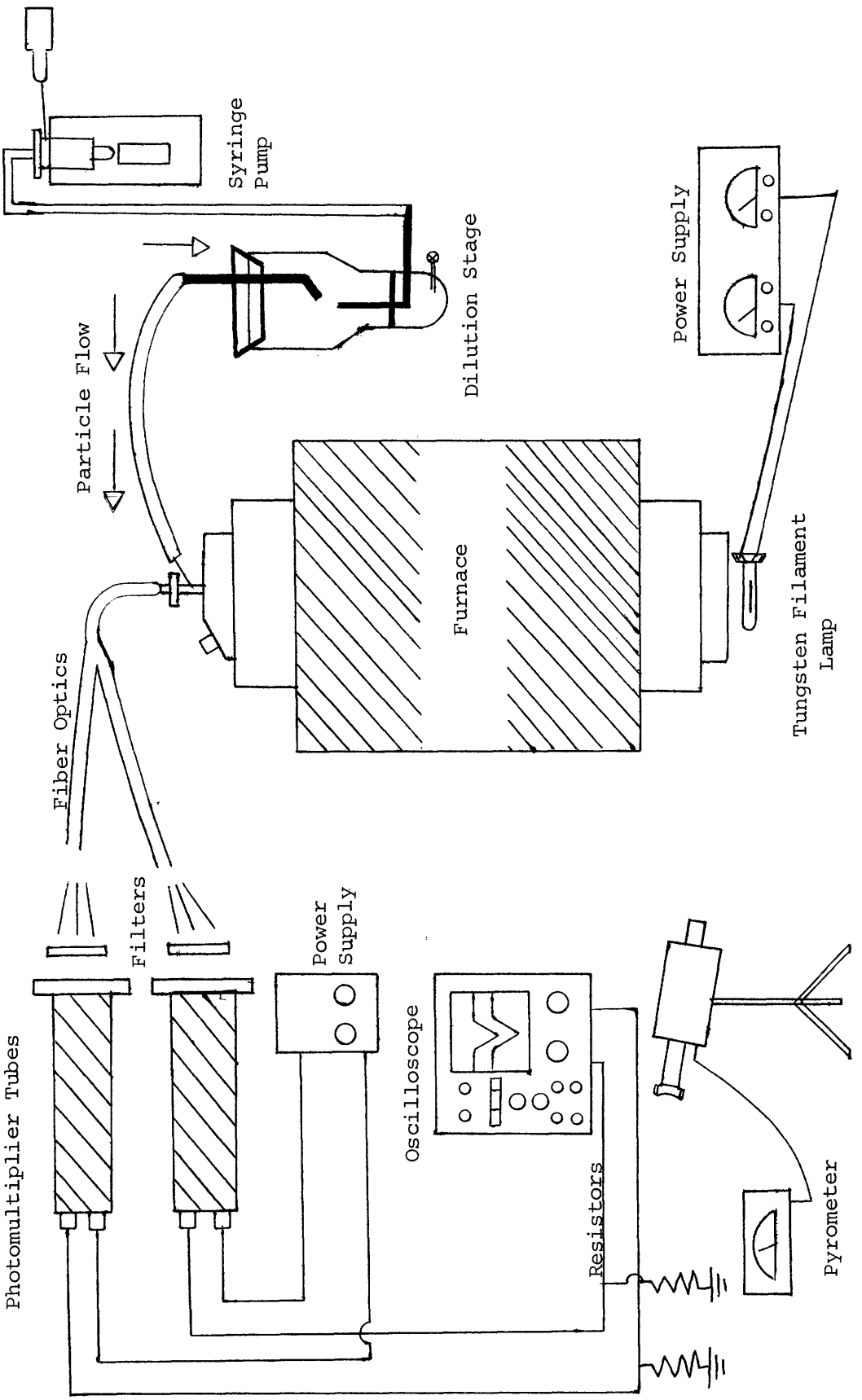

Figure 4.4: Schematic of Entire Operating System

necessary to change the voltage on the PMT's and refill the coal vial. Early in the experimentation it became apparent that drift was a problem. The schedule was changed to allow for calibrations immediately preceeding and immediately following the picture taking (gathering of temperature data). Calibration was not important for measuring burnout times.

The Pyro Micro-Optical Pyrometer was used to measure furnace temperature by viewing the alumina muffle tube through the side port. The brightness temperature is recorded throughout the remainder of this thesis; no emissivity corrections were made. Previous measurements using thermocouples have shown good agreement between gas and wall temperatures.

CHAPTER V

Results

A wealth of information can be obtained from every single burnout signal. Not only can one determine the temperature history of the individual particle during the course of its burnout, but also a statistical average of several particles (burning under similar conditions) may be made. It is important to treat the individual particle and the average or 'typical' particle separately since many variations between particles are likely to exist (e.g. size, ash content, volatiles, etc.).

5.1 Single Particle Burnout

All of the raw data in this study was in the form of two traces on the screen of a storage oscilloscope. Polaroid pictures were made of those traces that were to be interpreted into time-temperature histories. Other traces were used only to gather burnout time data.

Figure 5.1 contains four sets of traces that were typically viewed on the oscilloscope. The signals were inverted and appear here as they did on the oscilloscope. Time increases from left to right. Figure 5.1a shows thin clean traces and straight, distinct baslines. Such a signal is typical of a particle burning in an oxygen-rich environment

Figure 5.1a: Traces from a particle burning in an oxygen rich environment.

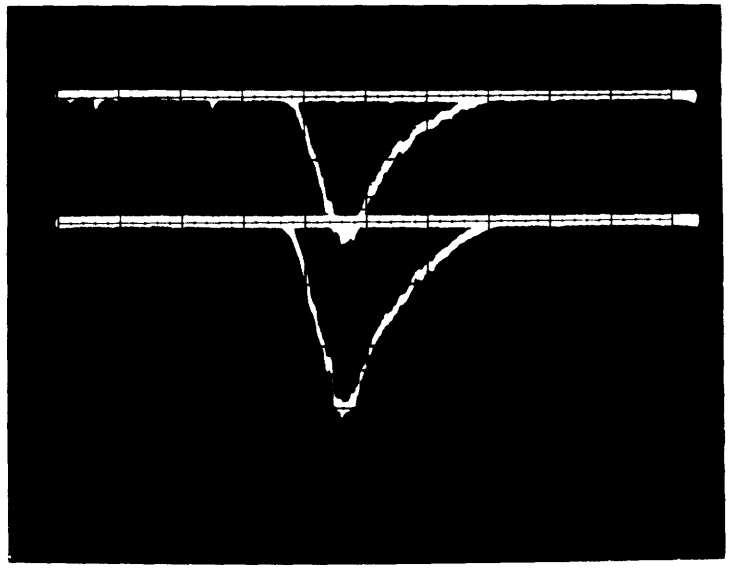

Figure 5.1b: Oscillating intensities.

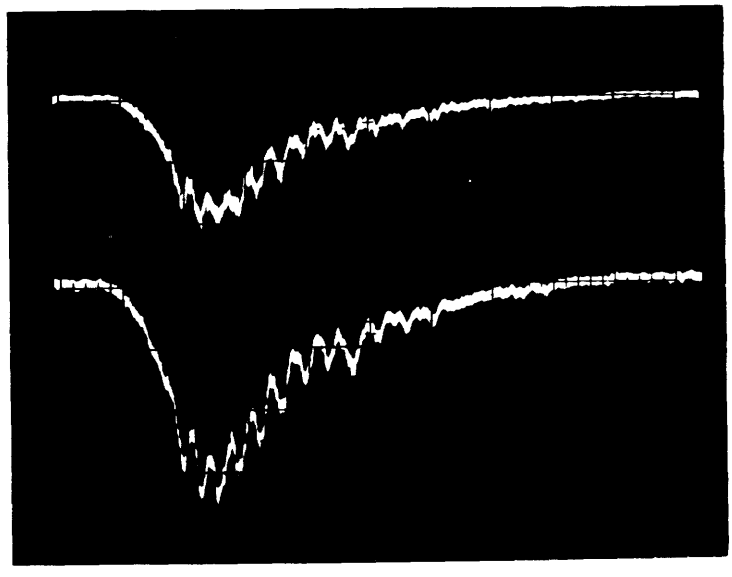

Figure 5.1c: Low signal-to-noise ratio typical of particles burning in low oxygen partial pressure.

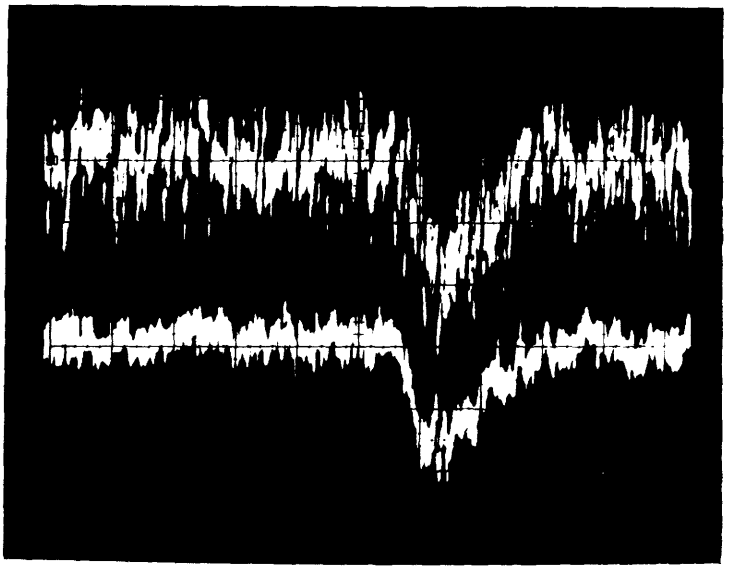

Figure 5.1d: Superimposed traces.

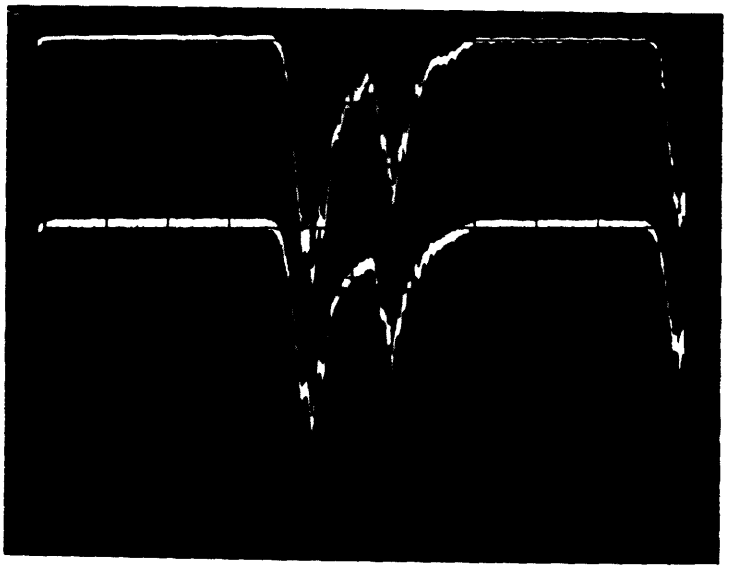

where the temperature is high. The burnout time is measured as the width of the lower peak at its baseline.

Oscillating intensities can be seen in Figure 5.1b. There exists at least three possible explanations for the oscillations: *i*) temperature is fluctuating; *ii*) the particle rotates exposing different surface areas to the detectors; *iii*) the particle is wavering in and out of the field of view. The profiles from several pictures were examined to see if *i* was true. No correlation was seen between absolute intensity and temperature even though temperature itself did fluctuate. Since

$$I \propto \frac{\text{surface area}}{\exp\left(\frac{C2}{\lambda T}\right) - 1}$$

one can correct for temperature change and deduce the ratio of surface areas should the particle be rotating as stated in *ii*. Neglecting further corrections for shrinkage from reaction, it was found that the ratio of large area / small area of a particle could be at least as high as 3.5.

Figure 5.1c shows the traces from a particle burned in 30 percent oxygen in helium. This particle's temperature was much less than the previous ones; the signal-to-noise ratio is very low. In cases such as this, a curve was drawn through the middle of each trace. Measurements were made using this curve. The error introduced by this method was quite large.

Figure 5.1d was included to give the reader an example of a suspicious trace. It is likely that a second particle ignited before the first had extinguished, and the signals from both appear as one on the oscilloscope. Traces such as these were not used to determine particle temperature.

Whenever possible, ten or more data points were determined for each burnout. For all but two particles at least five were taken. Figure 5.2 shows the temperature profiles for three typical particles. Sufficient data were collected to justify the smooth-curve approximations, but the purpose of providing this graph is to illustrate how temperature can vary within a single burnout. For all three particles there appears to be a rise-fall/rise-fall behavior for temperature although the trend in the middle curve might be an experimental artifact. The last peak in the top curve shows a 400 degree rise and fall that occurs in 4 milliseconds. The second peak in the bottom curve spans only 250 degrees and lasts 14 milliseconds.

The curves of Figure 5.2 are not representative of other profiles. Appendix D contains most of the temperature profiles reported in this thesis (B series excluded). The histories of several particles (from any one experimental condition) are plotted on each graph, and data points are connected by straight lines. This may be somewhat misleading, but it is the clearest and most concise representation of the full data set available. The representations in

Figure 5.2: Temperature Profiles of Individual Particles

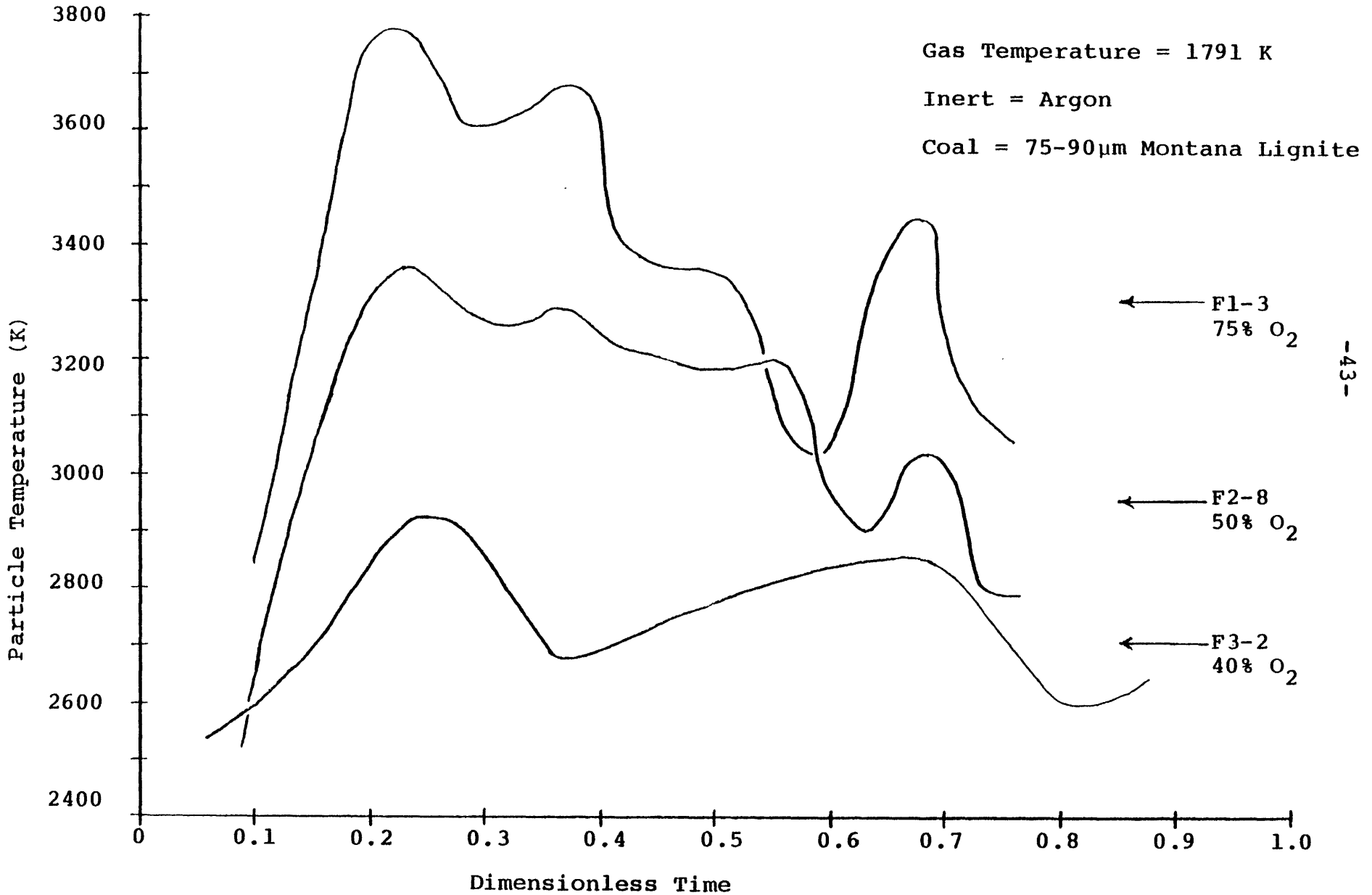

Appendix D should give the reader an idea of the variations that exist between particles for any one set of experimental conditions.

5.2 Average Behavior

Several runs were made to test the effects of oxygen partial pressure, ambient temperature, volatile content and initial particle size. A summary of all the experimental conditions is given in Table 5.1.

Average burnout times were calculated from approximately 100 traces except for E1 (n=46) and the B series. The physical properties listed in Appendix C were used to obtain the model-predicted burnout times shown in Figure 5.3. At 10 percent oxygen there is over a 2-fold difference between the calculated values and the data. Figure 5.4 compares the same values of Figure 5.3 with those from runs using helium. Three data points from argon systems at a lower gas temperature (G series) have also been plotted. These values fall on the original argon curve suggesting that the 255 K drop in gas temperature from 1791 K had little or no effect on burnout time.

The large spread in burnout times both within a run and between runs prompted the move to dimensionless time. The values of dimensionless time range from 0 to 1, so intervals between these extremes were used for calculating average temperatures. A computer program was written that separated

TABLE 5.1

Summary of Experiments

Run	% O_2	Inert	Temperature (K)	Particle	Particle Diameter (μm)
B1	100%	--	1753 K	Coal	90-105μm
B2	50	He	1753	Coal	90-105
B3	35	He	1753	Coal	90-105
B4	20	He	1753	Coal	90-105
E1	100	--	1791	Coal	75-90
E2	75	He	1791	Coal	75-90
E3	50	He	1791	Coal	75-90
E4	40	He	1791	Coal	75-90
E5	30	He	1791	Coal	75-90
F1	75	Ar	1791	Coal	75-90
F2	50	Ar	1791	Coal	75-90
F3	40	Ar	1791	Coal	75-90
F4	30	Ar	1791	Coal	75-90
F5	20	Ar	1791	Coal	75-90
F6	10	Ar	1791	Coal	75-90
G1	100	--	1536	Coal	75-90
G2	50	Ar	1536	Coal	75-90
G3	30	Ar	1536	Coal	75-90
J1	100	--	1536	Char	75-90
J2	100	--	1536	Coal	75-90
K1	100	--	1536	Coal	90-105
K2	100	--	1536	Coal	45-53

Figure 5.3: Burnout Times vs. O_2 Partial Pressure in an O_2-Ar System

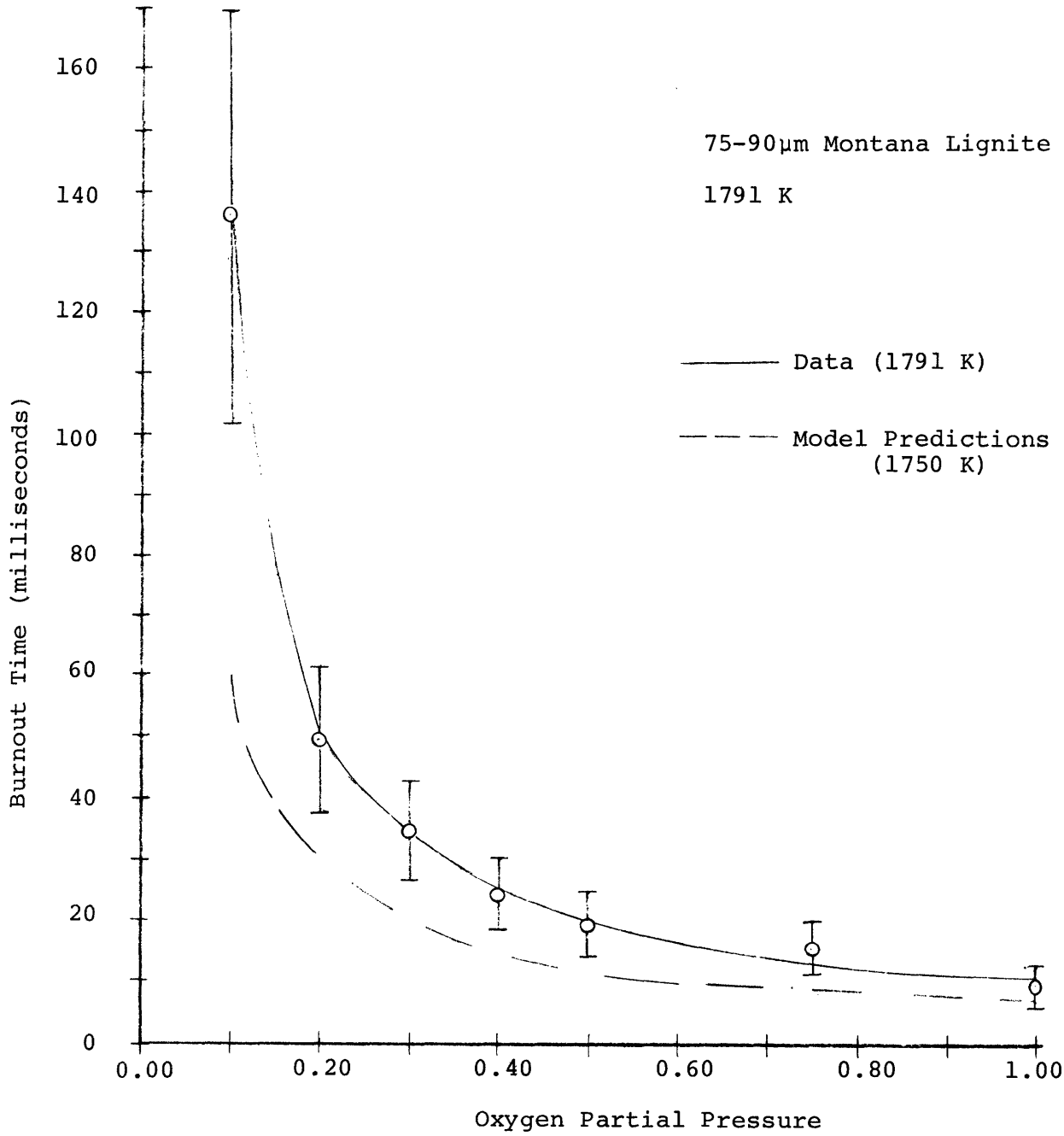

Figure 5.4: Comparison of Burnout Times

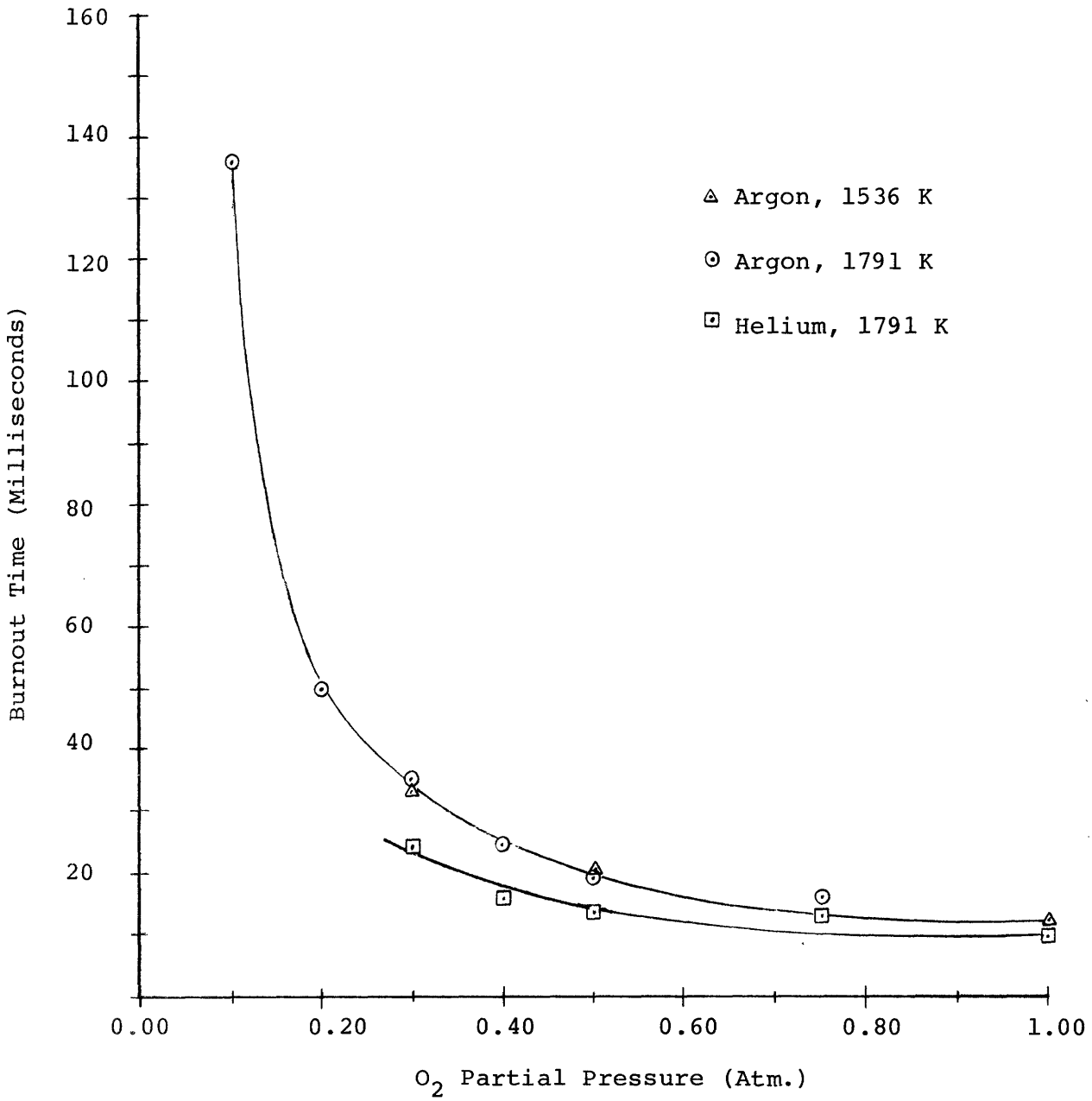

all of the data into five time intervals, averaged them and calculated standard deviations. The results of all of the runs are presented in Table 5.2. Time increases as one moves across the table, and for the B,E,F and G series, oxygen partial pressure decreases as one reads down a column.

Figure 5.5 compares the averaged results of runs F1, F4 and F6 with profiles predicted by the model. Standard deviations are reported in Table 5.2. The rise-fall behavior of temperature disappears as the oxygen partial pressure decreases. At low oxygen partial pressures temperature appears to increase monotonically with time as predicted by the model. At high oxygen concentrations the model incorrectly predicts both the temperature and the temperature profile. It is obvious from Figure 5.5 that there is no one point in (dimensionless) time at which temperatures should be compared; the temperature behavior is very different in each case. For this reason, caution should be applied when looking at Figures 5.6 and 5.7. These graphs represent the overall averages of all the data points at any given condition. The strong dependence of temperature on time at high oxygen concentrations is reflected in the large standard deviation. The model predictions have also been plotted and are much less accurate in predicting behavior in helium systems than in argon systems. Note that temperatures in argon systems approach the temperature at 100 percent oxygen

TABLE 5.2 Averages of Temperatures for Five Dimensionless Time Intervals

Run	Average Burnout Time	Dimensionless Time Interval 0-0.20	0.20-0.40	0.40-0.60	0.60-0.80	0.80-1.00
B1	--	3313 ±346	3450 ±250	3245 ±276	3090 ±272	--
B2	--	2580 ±234	2720 ±215	2703 ±137	2742 ±168	2654 ±146
B3	--	2285 ±191	2411 ±220	2427 ±124	2469 ±175	2466 ±163
B4	--	2038 ±144	2138 ±154	2143 ±133	2195 ±263	--
E1	9.6 ±3.3	3170 ±158	3316 ±140	3155 ±139	3177 ±250	--
E2	13.0 ±3.3	2745 ±213	3023 ±228	2905 ±244	2845 ±245	2728 ±500
E3	13.5 ±3.5	2470 ±176	2667 ±141	2846 ±197	2795 ±288	2932 ±316
E4	15.9 ±4.2	2491 ±279	2541 ±162	2566 ±191	2611 ±159	2742 ±367
E5	24.6 ±7.4	2271 ±165	2390 ±210	2345 ±208	2350 ±245	2516 ±224
F1	15.8 ±3.9	2940 ±366	3363 ±174	3225 ±135	3113 ±111	--
F2	19.5 ±5.4	2718 ±272	3000 ±175	2966 ±152	2925 ±180	2912 ±99
F3	24.5 ±5.8	2704 ±190	2932 ±103	2947 ±127	2880 ±120	2844 ±217
F4	34.9 ±8.2	2632 ±193	2741 ±136	2828 ±149	2786 ±189	2709 ±251
F5	50.0 ±12.0	2285 ±144	2422 ±139	2479 ±119	2497 ±127	--
F6	136 ±34	2146 ±126	2182 ±106	2255 ±150	2344 ±108	--
G1	12.5 ±3.4	3183 ±256	3365 ±298	3207 ±217	3175 ±204	--
G2	20.4 ±5.3	2862 ±227	3070 ±204	2945 ±180	2763 ±216	--
G3	33.7 ±7.9	2624 ±160	2688 ±174	2709 ±167	2759 ±179	2700 ±300
J1	10.4 ±4.4	3907 ±354	3941 ±360	3675 ±345	3606 ±384	3540 ±414*
J2	8.3 ±3.2	3417 ±531	3812 ±419	3485 ±481	3255 ±334	--
K1	10.7 ±5.6	3548 ±427	4014 ±318	3782 ±365	3542 ±320	--
K2	5.3 ±1.7	3421 ±309	3580 ±216	3477 ±263	3238 ±278	2909 ±105

* Originally 3835 ±680 before point T = 4719 K was removed.

Figure 5.5: A Comparison of Experimentally Determined Temperature Profiles with Model Predictions

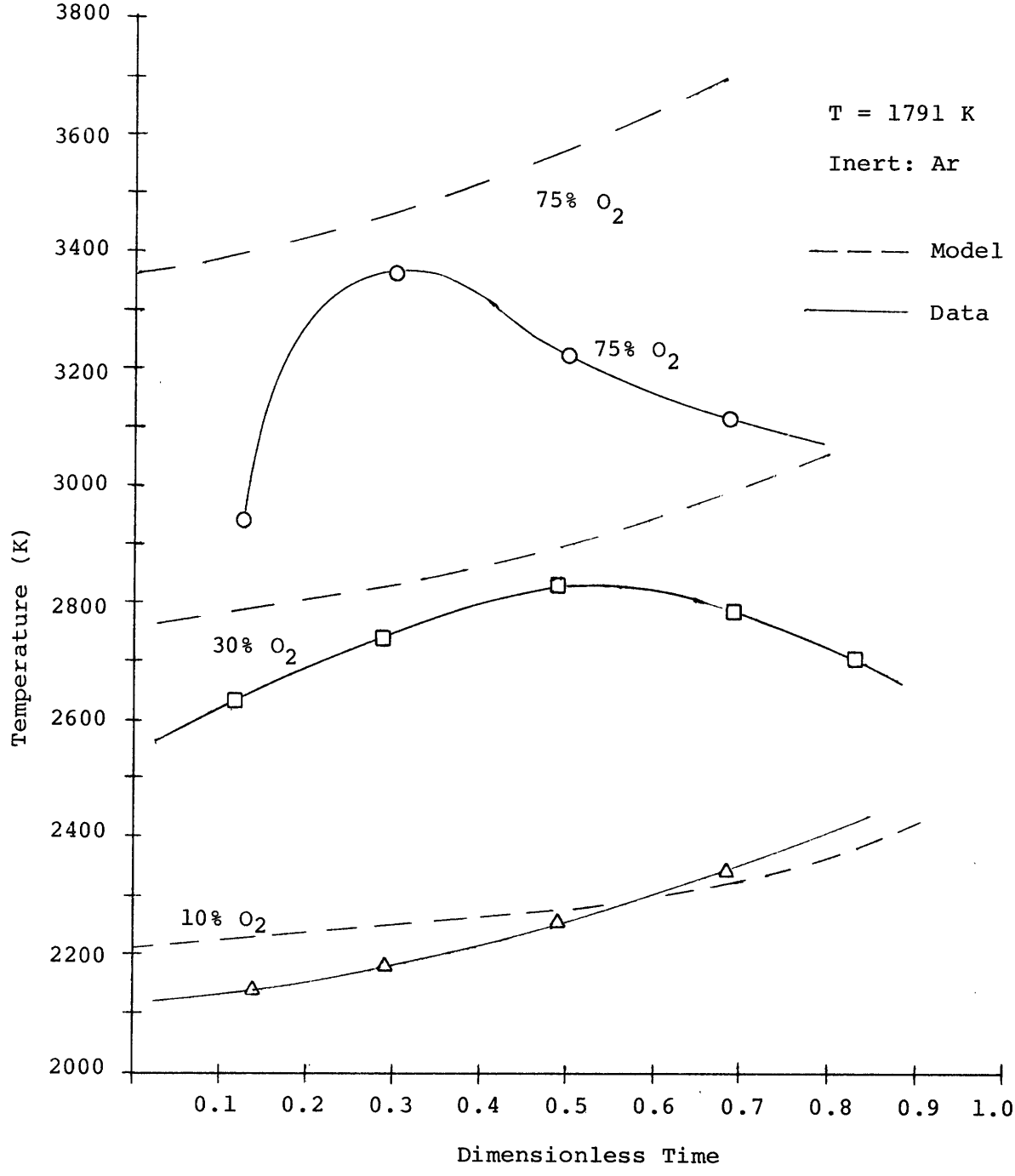

Figure 5.6: Average Temperatures vs. O_2 Partial Pressure in a He-O_2 System

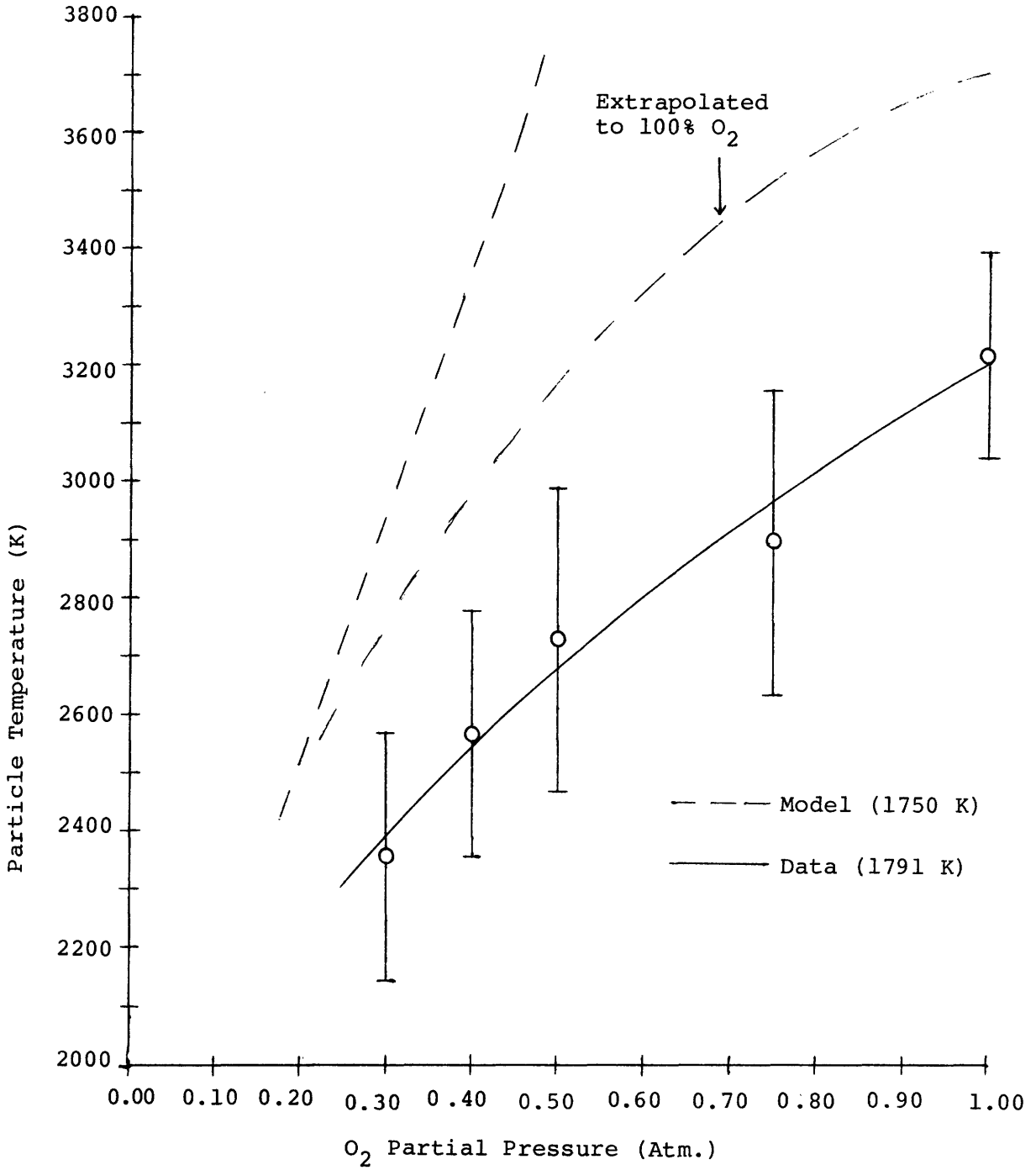

Figure 5.7: Average Temperatures vs. O_2 Partial Pressure in an Ar-O_2 System

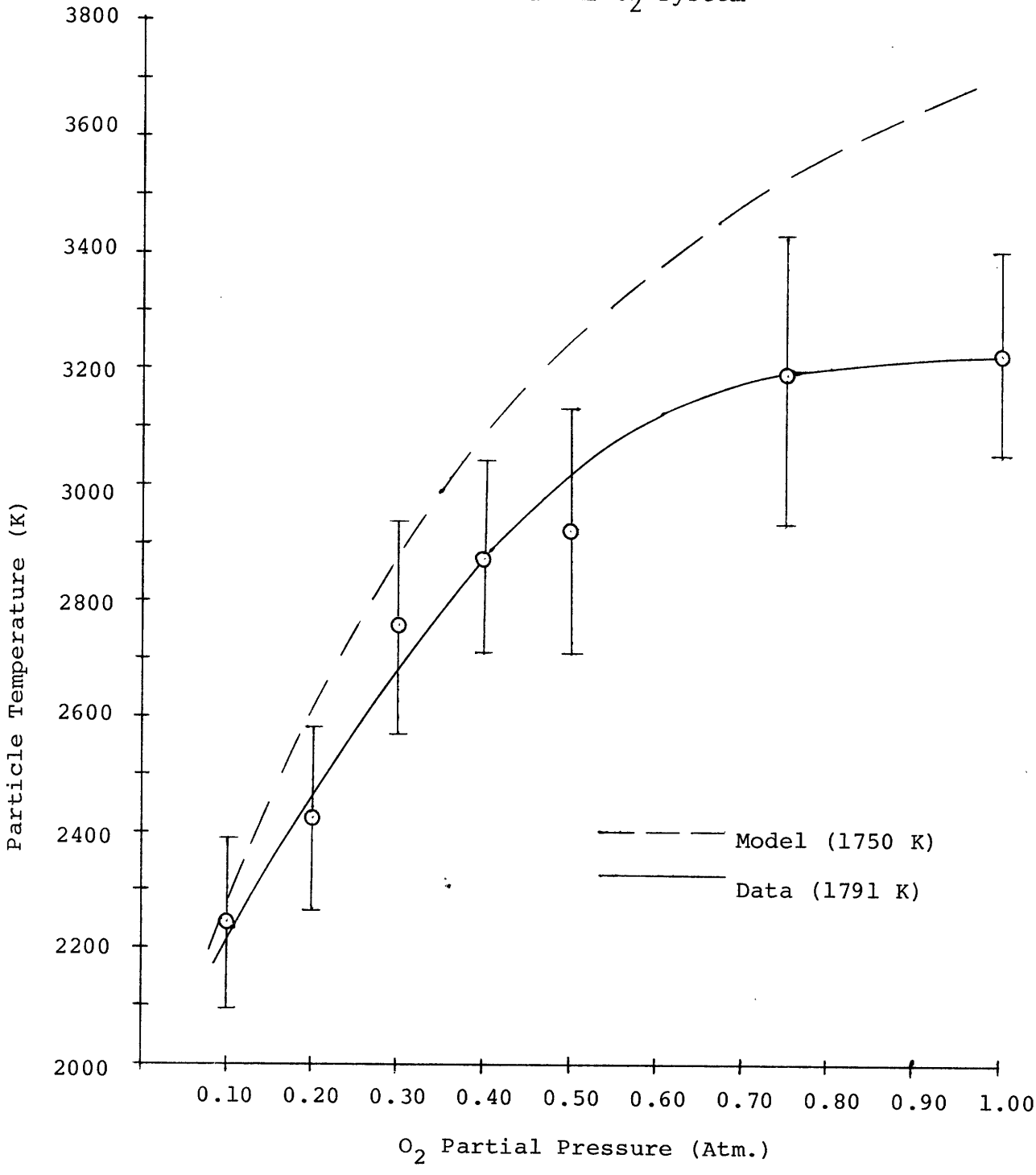

asymptotically whereas temperatures appear to fall sharply with a small dilution by helium.

The E and F series are fully plotted as functions of both oxygen partial pressure and dimensionless time in Figures 5.8 and 5.9. At all oxygen concentrations temperatures are higher in the argon systems than in the helium systems. The particle temperatures for 75 percent oxygen in argon appear to be higher than those of pure oxygen, but the overall average shown in Figure 5.7 is slightly lower. The temperature profile changes with decreasing oxygen concentration in the presence of either inert gas. At high concentrations the rise-fall behavior appears as noted earlier, and at low concentrations temperature increases in the course of a single burnout. At a given oxygen concentration, particles in argon burn hotter and slower than particles in helium.

The J series in Table 5.2 is a comparison between coal and char in 100 percent oxygen. The char was produced by purging Montana Lignite with an inert gas for one hour at 1000 C. The coal sample used in this run was different from that used in the E, F and G series. Figure 5.10 illustrates the difference in temperature profiles. The rise-fall behavior is again seen with the coal, but the rise is not clearly seen in the case of char. The average burnout time for char was 26 percent longer than that for coal. It should be noted that the standard deviations for burnout

Figure 5.8: Average Temperature Profiles
(E Series)

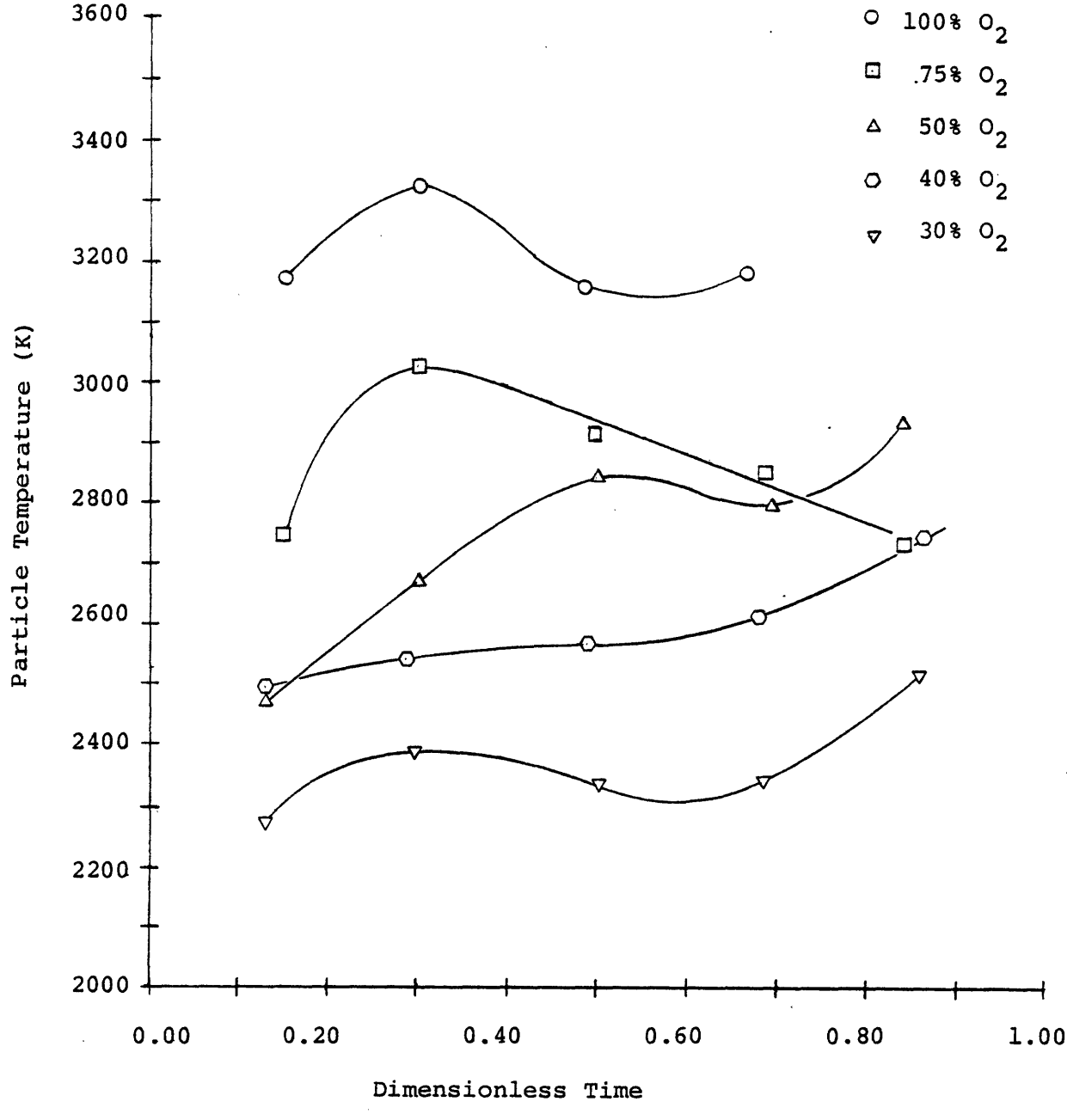

Figure 5.9: Average Temperature Profiles
(F Series)

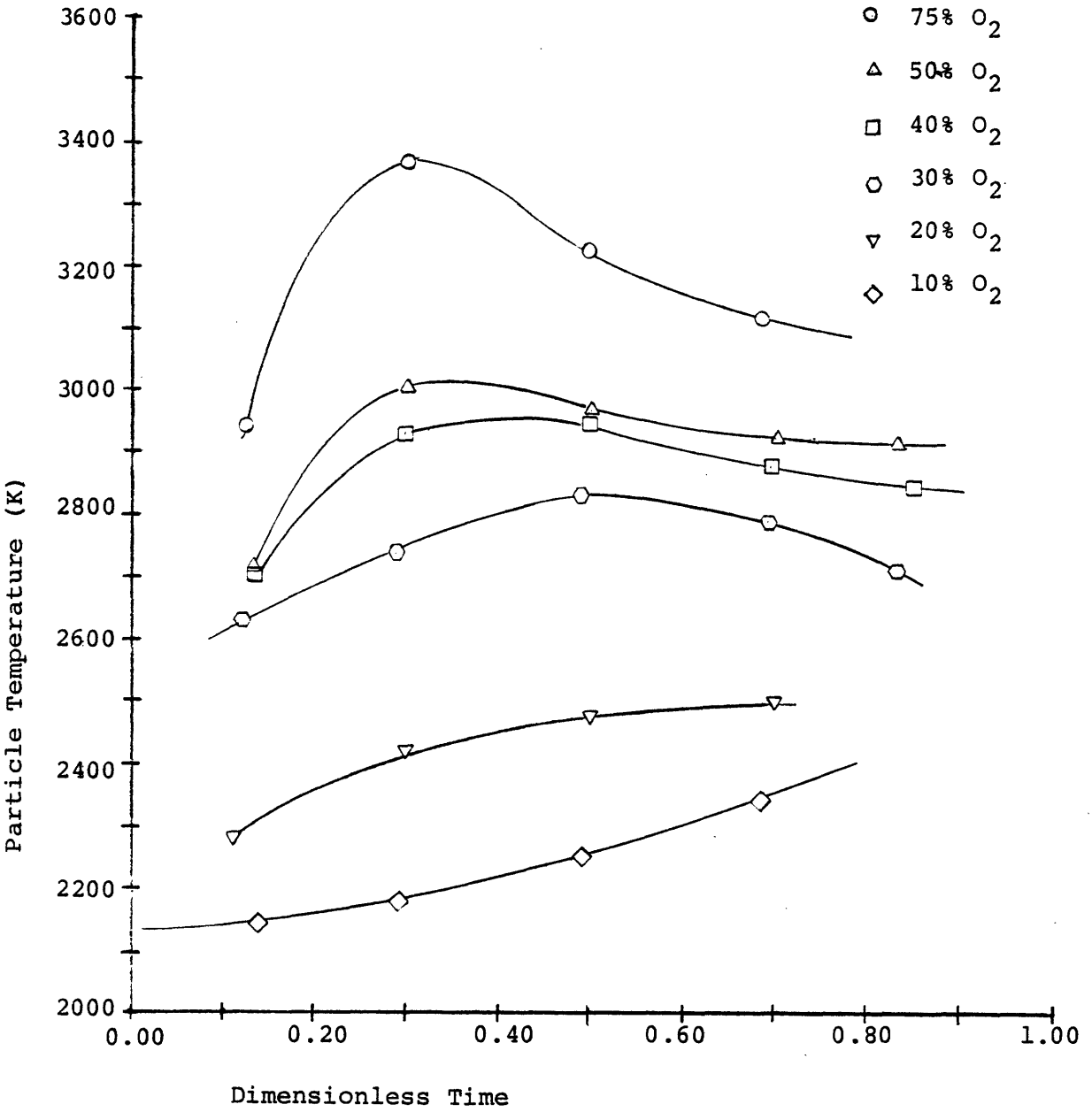

Figure 5.10: Char vs. Coal in 100% O_2

(J Series)

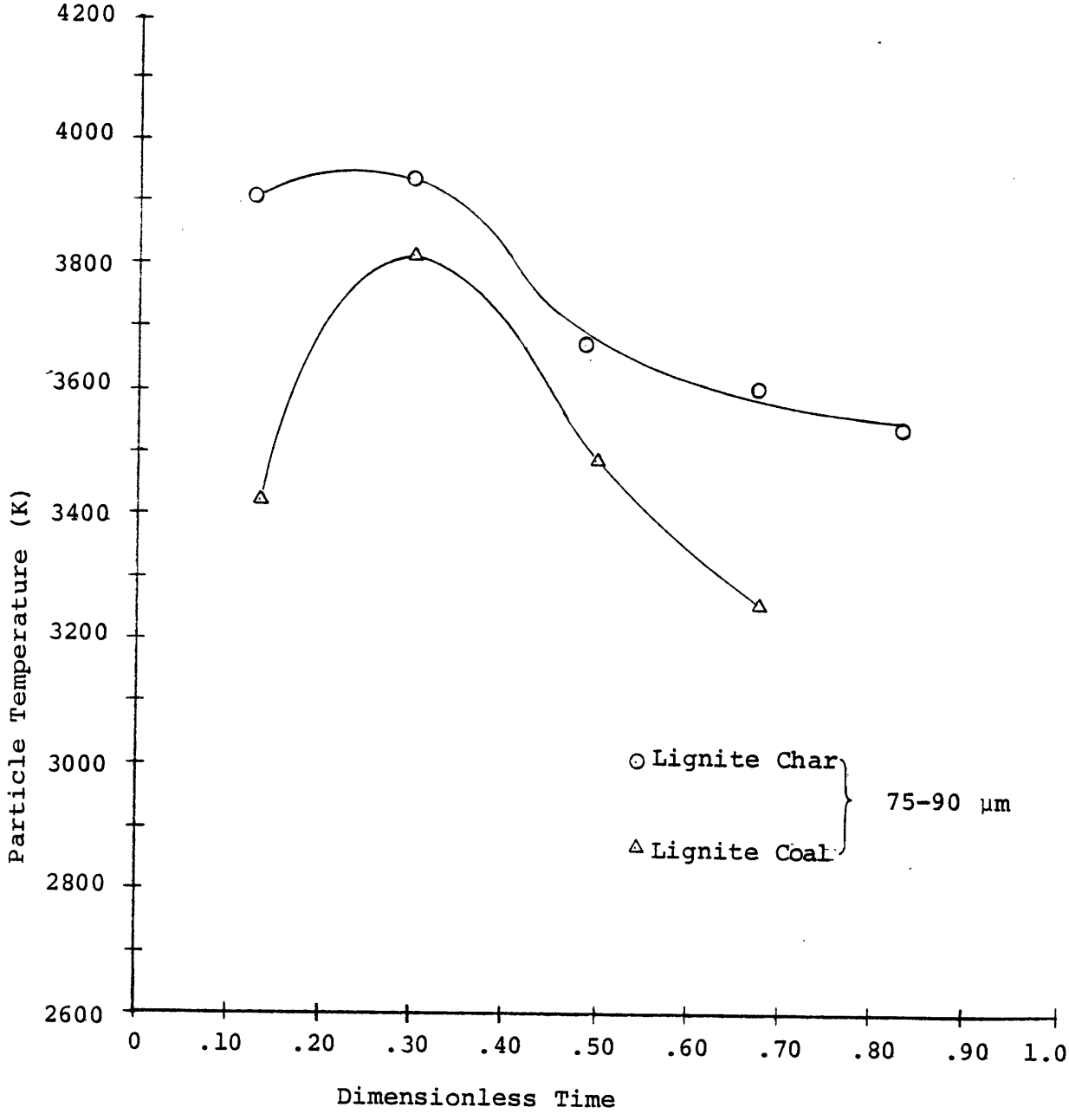

times were approximately 40 percent of the averages.

The K series tests for the effects of particle size in 100 percent oxygen. One again sees (by reading across Table 5.2) the rise-fall temperature behavior. The 90-105 μm fraction burns hotter than the 45-53 μm fraction. This is consistent with the steady-state assumptions coupled with the results for high oxygen partial pressures in the E, F, and G series. Temperatures are higher than expected from the results of E1, but burnout times are consistent with that same run.

5.3 Error Analysis

The interference filters used for all of the runs transmitted light at 450 and 550 nm, so equation (4.6) becomes

$$T = \frac{-5818.2}{\ln\left(\frac{I_{450}}{I_{550}}\right) - \text{constant}} \qquad (5.1)$$

The constant is actually the natural logarithm of the calibration constant of equation (4.5). It's value was typically between 0.30 and 0.45. Except for the B series, the standard deviation of any one set of calibrations was approximately 5 percent of the absolute value of the average constant. Drift between calibrations was often of the order of 10 percent. The uncertainty from the calibrations is obviously greater for high temperatures than for low ones. The effect

of drift is less than it appears to be simply because data were taken during the drift, and the results were averaged. That is to say, the low values for the constant partially cancelled the high values. Calibrations had no effect on burnout time measurements. Similarly, the drift of the constant is much slower than the burnout of a fuel particle. Temperature behavior within a single burnout is accurately determined, but the absolute value of the temperature is still dependent on the constant.

The greatest source of error arises in measuring intensities from a Polaroid photograph. The author could reproduce measurements within 1 or 2 percent, but this did not assure that the correct values were being determined. Ignition was often so rapid that the slope of the peak was too large to allow for highly accurate measurements. At the tail end of the burnout the particle is small and the signal low, and it is again very difficult to extract a highly accurate reading. Very few measurements were made between dimensionless times of 0.8 and 1.0. Highly noisy signals, such as those from runs with low oxygen partial pressures, were measured in a manner described previously in section 5.1.

Neglecting any of the smaller errors that may have arisen in the course of gathering and analyzing data, the author estimates an overall error in temperatures of 30 to 70 Kelvin degrees.

Burnout times were measured as the width of the 550 nm

peak at its baseline. The precision of the measurement depended on the sweep time setting of the oscilloscope. One difficulty encountered was the bias on the part of the operator. Although all peaks were used for burnout time data, only peaks that could easily be measured were used for temperature studies. The average burnout time of these peaks tended to be greater than the overall average. Conversely, though, the sweep time was usually set to produce the clearest peaks for any one run. Long burnouts did not fit the oscilloscope screen and had to be discarded. Modifications of the data acquisition system would have to be made to eliminate these problems.

CHAPTER VI

Discussion

The combustion model does not accurately predict temperature behavior for singly burning pulverized fuel particles. Its fit to experimental data is best at low oxygen concentrations (low temperatures), but this may be because experimentally determined and model predicted temperatures must each approach the furnace temperature at zero percent oxygen. Hence, they approach one another. There are other reasons for the large discrepancies at high temperatures, so it behooves us to return to the model's simplifying assumptions listed in Chapter III.

The first assumption is that the volatiles are instantly released and burned, and only a residual char remains to be oxidized. This may be a good assumption at high temperatures and low oxygen partial pressures where volatiles may burn for several milliseconds [6]. At high oxygen concentrations the total burnout time is of the order of 10 milliseconds, so one might expect that volatiles do not burn in a time that is short relative to the burnout time at these conditions. The results of the J series (char vs. coal) show the 'rise' in the rise-fall temperature profile to be absent for char. If the temperature rise is due to burning volatiles as postulated here, then Figure 5.8 and 5.9 show

that volatiles are still burning at a time 30 percent into burnout. One would expect (if the carbon does not burn while volatiles are burning) burnout times of char to be about 70 percent of the values for coal, but the data do not support this. Further studies should be done to determine the validity of these burnout time data which show that char has an average burnout time 26 percent greater than coal. The effect volatiles have on ignition cannot be determined from the current set of data because of the low sensitivity the detectors have to particles at ignition temperature.

The reaction $CO + \frac{1}{2}O_2 \rightarrow CO_2$ is assumed to occur far enough away from the particle surface that particle temperature is unaffected by it. Its incorporation in the model would cause predicted temperatures to be even higher than shown in Chapter V unless one assumes that the reaction consumes oxygen traveling to the particle surface yet has no direct heat effect on the particle. The data do not test the validity of this assumption. Any treatment of carbon dioxide production in a combustion model must be rigorous.

Butler and Brokaw [4] show that the effective thermal conductivity resulting from oxygen dissociation may be 8.4 times as large as the thermal conductivity expected for molecular oxygen at 3850 K. At high oxygen concentrations many particle temperatures approach or exceed this temperature at which the effective thermal conductivity is at a maximum.

Oxygen dissociation may greatly enhance heat transfer at high temperatures, and a serious error is introduced by neglecting it.

Likewise, the values for diffusivity in House's model are those of a binary system (oxygen plus inert). The thermal conductivity of helium is approximately 9 times that of argon, yet the model predicts much higher temperatures for particles in $He-O_2$ systems than for those in $Ar-O_2$ systems. This paradox results from the use of binary diffusivities. In reaching the particle surface, oxygen must diffuse through both the inert and the combustion products. For helium systems, the resistance oxygen meets in traversing a boundary layer of carbon monoxide is greater than that given by $He-O_2$ diffusivities. The $Ar-O_2$ diffusivity is expected to closely approximate the true diffusivity largely because the atomic weight of argon is comparable to the molecular weights of oxygen and carbon monoxide. Hence, the diffusion-controlled reaction rate in a helium system is over estimated as are the predicted temperatures.

It is simple to look back on a model and see where its faults lie, but difficulty is encountered when one tries to explain real data.

The behavior of singly burning particles as shown in Figure 5.2 is considered real and is not due to experimental error. Consistent trends are seen in each of the temperature profiles although none of them are simple functions of time.

The author proposes three possible explanations for the erratic behavior:

i) As the particle shrinks a 'patch' of ash either forms or is suddenly exposed on a portion of the particle surface. The ash prevents oxidation in that region but still conducts heat away from the particle. The reaction rate drops along with the particle temperature and rises again when the ash flakes off.

ii) An uneven distribution of combustible matter with different heats of combustion exists within a single particle. During a burnout the amount of heat released by reaction varies.

iii) A lopsided pore size distribution may exist. The opening and exposure of large pores may decrease the reaction rate and reduce particle temperature. In the extreme, the particle may actually split, and the detectors suddenly view a particle of a different size.

Despite the unusual behavior of the individual fuel particle, consistent trends in average temperature profiles have been seen. The most notable observations is that particles burn hotter and slower in argon-oxygen atmospheres than in helium-oxygen environments. As mentioned earlier, this follows from the differences in thermal conductivity and diffusivity. The thermal conductivity of argon is less

than that of helium, so argon acts to trap heat at the particle surface. Argon also offers more resistance to diffusion; combustion products (and dissociated O_2) are held closer to the burning particle than in a helium system, and oxygen diffuses more slowly to the surface. The particle temperature may either increase or decrease on substituting helium for argon, depending on the relative magnitudes of the increases in mass and heat transfer to the particle. The data suggest lower temperatures with helium than with argon. The question of whether or not temperatures are higher in systems slightly diluted with argon than in pure oxygen should be resolved with further experimentation. Similarly, the rapid drop in temperature caused by small dilutions with helium should also be verified experimentally. The results of these investigations may be very useful for modeling purposes.

Temperature decreases at high oxygen partial pressures and increases at low ones during the course of a single burnout. One possible explanation of this behavior involves the oxidation of carbon monoxide to form carbon dioxide in a flame front about the particle. Field et al. [6] provide an interesting discussion on the locus of carbon monoxide burning. They report that carbon monoxide oxidation within the boundary layer is most significant for large particles and for small particles occurs primarily outside the boundary layer. This would explain the trend in temperature at high oxygen partial pressures.

The J series show that char burns significantly hotter than coal. Since the low-Btu volatiles are removed from char, the residual carbon structure has a higher heating value and therefore burns at a higher temperature. The reason coal temperatures do not approach those of char after the volatiles (of the coal) are released and burned is not well understood.

The effect of lowering the ambient temperature from 1791 K to 1536 K (G series) appears to be negligible. The burnout times at the lower temperature are in excellent agreement with those of the higher temperature. Also, the B series (which has a higher uncertainty associated with its calibration than any other run) is consistent with the E series regardless of the small difference in gas temperature. The B series runs as low as 20 percent oxygen in helium, but its particle size is different from most of the other experiments. The B1 and K1 runs should have produced similar results. The reason for the differences is yet to be explained; perhaps the coal sample had become contaminated in the period between these runs. This could explain the 52 percent standard deviation for the average K1 burnout time.

The effect of particle size on burnout time is qualitatively correct. The ratio of the squares of diameters for the 90-105, 75-90 and 45-53 micron fractions is 3.97:2.85:1, respectively. The data yield a ratio of burnout times of 2.06:1.85:1 (K1:E1:E2). This shows a smaller size effect

than predicted from a d^2 law (external diffusion). As expected from the steady-state approximations and preliminary results, the large particles burned hotter than the small ones in 100 percent oxygen.

CHAPTER VII

Conclusion and Recommendations

7.1 Conclusions

The temperature profile of a singly burning particle is somewhat erratic and not a simple function of time. Three proposals on why this might be so are offered: *i*) ash formation blocks reaction and behaves as a heat sink; *ii*) uneven distribution of combustible matter with different heats of combustion; *iii*) uneven pore distribution leading to particle fragmentation.

Data from the E and F series of experiments show that, for any given oxygen partial pressure, coal particles will burn slower and at a higher temperature when argon is used as the diluent inert gas than when helium is used. Particles in helium systems burn colder and faster because of larger diffusivities and thermal conductivities. Comparison of the data with the model suggest that oxygen dissociation and multicomponent diffusion must be considered in any working coal combustion model.

Particle temperatures in higher concentrations of oxygen first rise and then fall with time. As the oxygen partial pressure decreases, the magnitude of the rise-fall behavior diminishes. At low oxygen partial pressures, temperature monotonically increases with time. The 'rise'

in the rise-fall behavior is attributable to the release and burning of volatiles. Explanations for the temperature behavior at various oxygen concentrations might be found in models for the oxidation of carbon monoxide.

The effect of lowering gas temperature from 1791 K to 1536 K (brightness) was negligible with respect to temperatures and burnout times for argon systems. The temperatures of burning char exceed those of coal presumably because of the higher heating value of char. The temperatures of different particle size fractions burned in 100 percent oxygen are consistent with the behavior predicted by the (decreasing) temperature-time profile at that condition.

7.2 Recommendations Concerning Experimental Apparatus

The most important change that must be made in the system shown in Figure 4.4 involves the water-cooled feeder probe. The use of flat black paint on the inner surface did not prevent reflected light from the furnace walls from reaching the detectors. The high background rendered the system insensitive to particle temperatures below 2000 K. Ideally, all light should be blocked out so that the PMT output is due only to the dark current. Electroplating the inside wall of the feeder probe and mounting a non-reflective surface beneath the furnace may help reach that goal. The geometry of the system only requires that the bottom 2 1/2 inches of the probe be completely non-reflective. If that

were possible, the remainder of the tube could be coated with a reflecting surface to collect as much light as possible from the particle. This modification alone could result in a 12-fold gain in the amount of light recovered from a burning particle.

The data acquisition system should be modified to minimize operator input and reduce the error associated with data analysis (i.e. measuring intensities from a Polaroid photograph). One suggestion is to split the signals - electronically ratio the two intensities creating a single output and simultaneously monitor the signals on an oscilloscope. The single-channel output may be fed directly to a chart recorder or computer.

The sensitivity of many photomultipliers extends into the near infra-red region, but the light intensity gained by operating in this region is lost due to a lower quantum efficiency. Cooling the photomultipliers will be of little value unless light from the furnace walls is prevented from climbing the feeder probe. The same is true of using an amplifier.

7.3 Future Work

It is obvious now that House's model needs a good deal of refinement, or a more complex model needs to be developed. Considerable attention must be paid to the combustion products and their effects on heat transfer and diffusion. The

new model should be consistent with the data presented here as well as any new data collected. The parameters of the model will be useful in determining what further studies should be conducted. Some guidance is needed. Otherwise, the number of possible experiments increases without bound as one considers changing coal types, oxygen concentrations, inert gases, particle sizes and gas temperatures. In doing all of these experiments one also defeats the purpose of having a model.

Topics that are especially worthy of further study include:

i) Density Fractionation. The wide spread in both burnout time and temperature data may be partially due to differences in particle densities. Experiments can easily be performed to test for any correlations.

ii) Low Oxygen Concentrations. The work reported here does not cover oxygen concentrations below 10 percent in argon and 20 percent in helium. Work done at low oxygen concentrations will be useful for modeling purposes as well as on-going ash vaporization studies. At high concentrations it was assumed the particle burned completely; at low concentrations this assumption may no longer be valid.

iii) Effects of Volatile Matter. The comparison of char with coal in 100 percent oxygen is somewhat inconclu-

sive. Char burns at a higher temperature, but it was difficult to determine whether or not the 'early' temperatures in a coal burnout are due totally to volatiles. Studies comparing char with coal at lower oxygen concentrations are likely to be very informative. Similarly, a study should be made comparing chars devolatilized under different conditions.

iv) Ignition and Extinction. Rather than focus on the entire burnout, separate studies should be done on ignition and extinction. The effect of volatiles on ignition could be studied along with *iii*. Temperature behavior near extinction remains uncharacterized because of the lack of data between 0.8 and 1.0 dimensionless time.

v) Particle Size Distribution. The most obvious explanation for variations in burnout times is that it is the result of a particle size distribution. Before beginning studies with density-fractionated coal, it would be very worthwhile to search for correlations that may exist between size and burnout time distributions.

This list may not be complete, but it provides a foundation on which to build. A great deal of insight into the mechanisms and kinetics of combustion may be gained from the time resolved measurement of temperature during burnout.

APPENDIX A: NOTATION

c - speed of light (= 2.998×10^{10} cm/sec)

cD - diffusivity (moles/cm-sec)

C - calibration constant

C1 - Planck's 1st Radiation Constant (=3.74×10^{-12} watts-cm^2)

C2 - Planck's 2nd Radiation Constant (=1.44 cm-K)

C_{D1}, C_{D2} - Parameters for linear approximation of diffusivity

C_{H1}, C_{H2} - Parameters for linear approximation of heat of reaction

C_{K1}, C_{K2} - Parameters for linear approximation of thermal conductivity

h - Planck's constant (=6.624×10^{-27} ergs/sec)

ΔH_{rxn} - heat of reaction (cal/mole O_2)

I_i - measured intensity at wavelength i (watts)

k - thermal conductivity (cal sec^{-1} cm^{-1} K^{-1})

K - Boltzmann's constant (=3.2994×10^{-24} cal/K)

N_{CO} - molar flux of carbon monoxide (g-moles/cm^2-sec)

N_{O_2} - molar flux of molecular oxygen (g-moles/cm^2-sec)

q_λ - light intensity at wavelength λ(watts/cm^2)

Q - radiative heat loss (cal/sec)

r - radius from center of particle (cm)

r_{avg} - time-averaged radius of particle (cm)

r_p - particle radius (cm)

R - reaction rate (moles O_2/sec)

S - mass of carbon consumed by reaction per mole of O_2 (=24 g/mole for $2C + O_2 \rightarrow 2CO$)

$t_{b.o.}$ - burnout time (sec)

T - temperature (K)

T_b - brightness temperature (K)

T_t - true temperature (K)

T_p - particle temperature (K)

T_w - wall temperature (K)

T_∞ - bulk gas temperature (K)

X_{O_2} - mole fraction of O_2

$X_{O_2\infty}$ - mole fraction of O_2 in bulk

ϵ_i - emissivity of particle at wavelength i

$\eta_{L,i}$ - efficiency of carrying light of wavelength i

$\eta_{D,i}$ - efficiency of detector at wavelength i

λ - wavelength (cm)

$\Delta\lambda$ - bandwidth (cm)

ρ - density of burning particle (g/cm^3)

σ - Stefan-Boltzmann constant ($=1.355 \times 10^{-12} cal.sec^{-1}cm^{-1}K^{-4}$)

APPENDIX B - PLANCK'S LAW

The bandwidth of the filters may be increased to enhance the signal from the detectors. Rather than using a point-to-point ratio as shown by the dotted lines in Figure B-1 and given by equation (4.4) of the text, integrated 'bands' beneath the radiation curve must be used. Corrections must be made for filter transmission (part of η_L) and detector efficiency (η_D) so equation (4.4) becomes

$$\frac{I_A}{I_B} = C \cdot \frac{\sum_{\lambda_A - \frac{\Delta\lambda_A}{2}}^{\lambda_A + \frac{\Delta\lambda_A}{2}} \eta_{L,A}(\lambda)\eta_{D,A}(\lambda)\lambda_A^{-5} \exp\left(\frac{-C2}{\lambda_A T}\right)\Delta\lambda_A}{\sum_{\lambda_B - \frac{\Delta\lambda_B}{2}}^{\lambda_B + \frac{\Delta\lambda_B}{2}} \eta_{L,B}(\lambda)\eta_{D,B}(\lambda)\lambda_B^{-5} \exp\left(\frac{-C2}{\lambda_B T}\right)\Delta\lambda_B}$$

The functionalities of $\eta_{L,i}$ and $\eta_{D,i}$ must obviously be determined. If the bandwidths becomes too wide and begin to overlap one another, the sensitivity of I_A/I_B to temperature diminishes. The calibration constant (C) arises now from the geometry of the system.

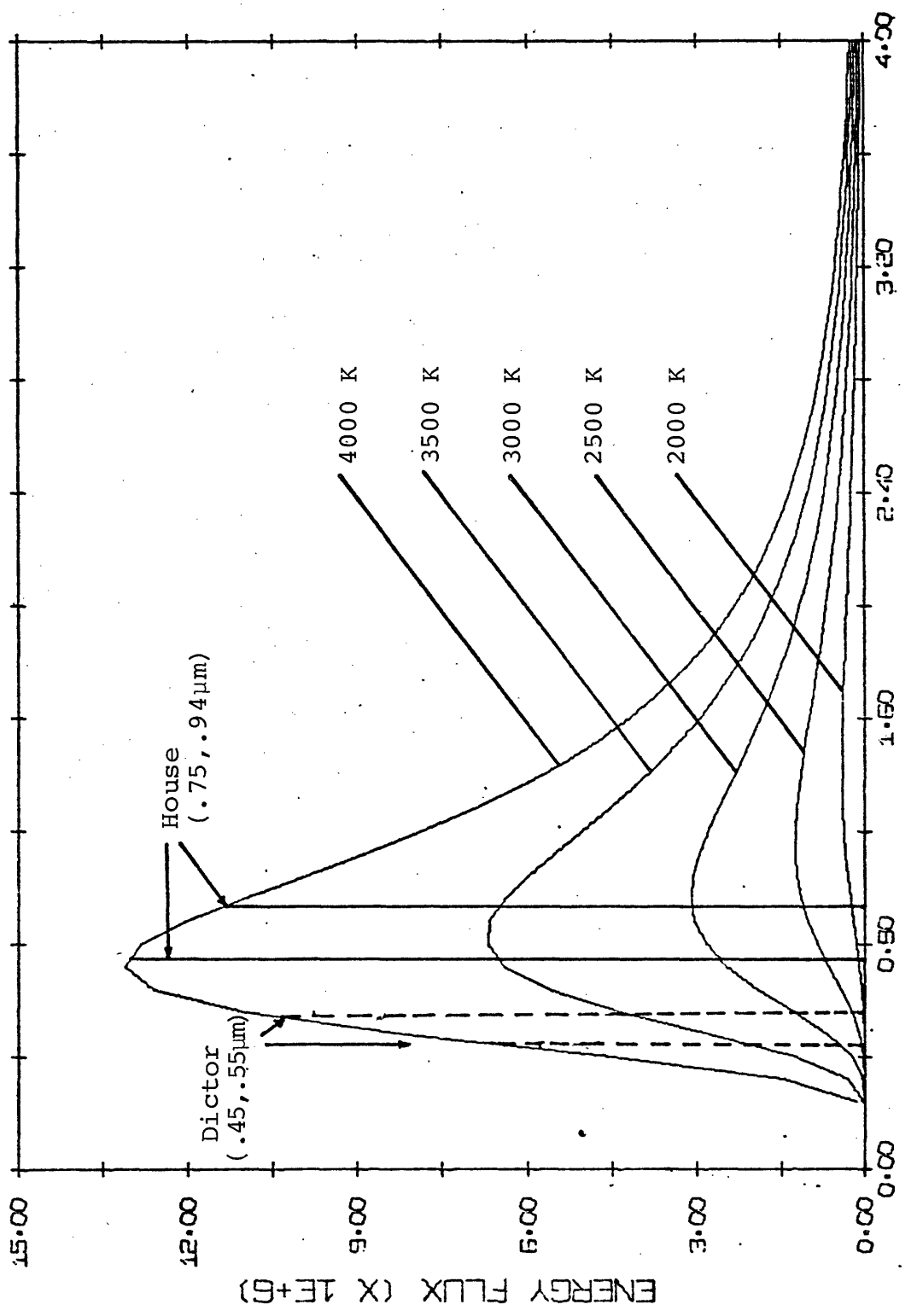

Figure B-1: Planck's Law

APPENDIX C - COMPUTER PROGRAMS

The following program was used to generate time-temperature profiles from the combustion model. The subroutine is basically House's original program except for the modifications described in the text. Given particle radius, oxygen mole fraction and gas and wall temperatures, the program will calculate burnout times and reaction rates for the shrinking sphere. It also prints and plots (on an IBM 1130) the temperature profile.

Thermal conductivity constants for equation (3.5) are arithmetically averaged in the program on the basis of oxygen mole fraction. These constants were found to be [9]:

TABLE C-1

	Ar	He	O_2
C_{K1}	4.73×10^{-5}	4.28×10^{-4}	5.35×10^{-5}
C_{K2}	5.88×10^{-8}	5.34×10^{-7}	1.19×10^{-7}

The units are cal $sec^{-1}cm^{-1}K^{-1}$. The Chapman-Enskog kinetic theory [3] was used to calculate diffusivities, and linear approximations of the results are given:

$$O_2\text{-Ar:cD} = 9.14 \times 10^{-9}T + 1.17 \times 10^{-5} \text{ moles } cm^{-1}sec^{-1} \quad \text{(C-1)}$$

$$O_2\text{-He:cD} = 3.70 \times 10^{-8}T + 3.07 \times 10^{-5} \text{ moles } cm^{-1}sec^{-1}$$

The heat of reaction used was

$$(-\Delta H_{rxn})_T = 49740 + 3.64T \quad \text{cal/g-mole } O_2 \qquad \text{(C-2)}$$

This equation is for the formation of carbon monoxide only.

The next program was used to process raw data. The user provides all of the time/intensity data along with a calibration constant, and the computer outputs time-temperature profiles both in print and on a plot (IBM 1130).

```
      SUBROUTINE KEITH(TEMP,HRATE,RP,TW,TP,TINF,PRESS,RATE1,FINO2)
C
C
C     MASS TRANSFER GOVERNED COMBUSTION MODEL FOR COAL PARTICULATES
C
      DIMENSION RATE(100)
C    CH1 AND CH2 ARE THE PARAMETERS FOR THE LINEAR APPROXIMATION FOR
C    THE HEAT OF REACTION.
      CH1=49740.
      CH2=3.64
C    CD1 AND CD2 ARE THE DIFFUSIVITY CONSTANTS.
      CD1=3.07E-5
      CD2=3.7E-8
C    CK1 AND CK2 ARE THE THERMAL CONDUCTIVITY CONSTANTS.
      CK1=XO2*5.35E-5+(1.-XO2)*4.28E-4
      CK2=XO2*1.19E-7+(1.-XO2)*5.34E-7
      RATE(1)=RATE1
C   F IS THE PERCENT ACCURACY/100 AT WHICH THE BELOW ITERATION QUITS
      F=.001
      PI4=12.566
      SIGMA=1.355 E-12
      DELTA=256.
      XO2=PRESS
C    THE NEXT FEW LINES CALCULATE THE RATE GIVEN BY THE HEAT BALANCE.
7     QRAD=PI4*SIGMA*(TP**4-TW**4)*RP*RP
      A=4.*3.14159*RP*CK1/CH2
      B=4.*3.14159*RP*CK2/CH2
      DO 10 N=2,300
      C=(QRAD/RATE(N-1)-CH1)/CH2
      D=CH1+CH2*TP-QRAD/RATE(N-1)
      E=CH1+CH2*TINF-QRAD/RATE(N-1)
      RATE(N)=(A+B*C)*ALOG(D/E)+B*(TP-TINF)
      DUMMY=ABS(RATE(N))
      RATE(N)=(DUMMY+RATE(N-1))/2.
      FRAC=ABS(DUMMY-RATE(N-1))/RATE(N)
      IF(FRAC.LT.F)GO TO 20
10    CONTINUE
      GO TO 999
20    HRATE=RATE(N)
      RATE(1)=HRATE
C    THE FOLLOWING LINES USE THE RATE EXPRESSION GIVEN BY SOLUTION
C    TO FICK'S LAW.  AFTERWARDS, A CHECK IS MADE TO SEE IF THE EXPRESSION
C    YIELDS THE CORRECT VALUE FOR THE BULK OXYGEN PARTIAL PRESSURE.
      A=(HRATE*CK2/4./3.14159/CD2)/(RP*(CK1*(TINF-TP)+CK2*(TINF*TINF-TP*
     1TP)/2.))
      B=CK1/CK2-CD1/CD2
      C=CD1+CD2*TINF
      D=CD1+CD2*TP
      VLOG=A*(B*ALOG(C/D)+TINF-TP)
      VLOG=-VLOG
      PO2=(1./EXP(VLOG))-1.
      IF(PRESS.EQ.0.)  GO TO 60
C   ITERATION PROCEDURE TO ZERO IN ON THE DESIRED VALUE FOR 'PRESS'
      IF(PO2.GT.PRESS) GO TO 50
      TP=TP+DELTA
      GO TO 7
50    TP=TP-DELTA
      DELTA=DELTA/2.
      IF(DELTA.EQ.1.) GO TO 60
      GO TO 7
60    CONTINUE
      TEMP=TP
      FINO2=PO2
      RETURN
999   WRITE(3,998)
998   FORMAT(' YOU BLEW IT - THE ITERATION DID NOT CONVERGE OR THE
     1 NUMERICAL INTEGRATION IS TAKING TOO MANY STEPS')
      RETURN
      END
```

```
      THIS PROGRAM IS DESIGNED TO DETERMINE FULL TIME/TEMPERATURE HISTORIES
       ; COMBUSTING COAL PARTICLES USING THE MODEL DEVELOPED BY KEITH
      HOUSE.  HIS ORIGINAL PROGRAM, WHICH IS USED HERE AS A SUBROUTINE,
      HAS BEEN SLIGHTLY MODIFIED.  FIRST, THE NUMERICAL INTEGRATION
      THAT ARISES FROM THE DIFFUSION EQUATION IS GIVEN A CLOSED-FORM
      SOLUTION.  SECOND, THE APPROXIMATION ORIGINALLY USED OF THERMAL
C     CONDUCTIVITY = CONSTANT*TEMPERATURE IS NOW OF THE FORM K=AT+B.
C     MOST OF THE PROGRAM REMAINS UNCHANGED.
C
C
        REAL XTITL(5),YTITL(5),KTITL(5),KEY1(3),KEY2(3),KEY3(3),KEY4(3)
        DIMENSION RP(15),TIME(15),TP(15),REALR(15),RLTIM(15),DLST(15)
        DIMENSION RATE(15)
        DATA KTITL/'GAS-','WALL',' TEM','PERA','TURE'/
        DATA XTITL/'DIME','NSIO','NLES','S TI','ME  '/
        DATA YTITL/'PART','ICLE',' TEM','PERA','TURE'/
        DATA KEY1/'   2','000 ','K   '/
        DATA KEY2/'   1','750 ','K   '/
        DATA KEY3/'   1','500 ','K   '/
        DATA KEY4/'   1','250 ','K   '/
        CALL PSKIP
        CALL LINSQ(3,0,0.0,3000.,1.0,5500.,XTITL,YTITL)
        CALL KEYSQ(1,4,KTITL,KEY1,KEY2,KEY3,KEY4)
        DUMMY=0.
        IJK=0
C     READ GAS TEMPERATURE,WALL TEMPERATURE,PARTICLE RADIUS,OXYGEN
C     PARTIAL PRESSURE(MOLE FRACTION)
1       READ(2,10)TINF,TW,RPO,PRESS
10      FORMAT(2F10.0,F10.7,F10.5)
        IF(TINF.EQ.0.0) CALL EXIT
        RMICR=10000.*RPO
        XO2=PRESS
        WRITE(3,12)RMICR,TINF,TW,PRESS
12      FORMAT('1','INITIAL RADIUS =',F6.2,' MICRONS'/' GAS TEMPERATURE ='
       1,F6.0,' K'/' WALL TEMPERATURE =',F6.0,' K'/' FRACTION OXYGEN =',F5
       2.3////)
        WRITE(3,15)
15      FORMAT(' ',9X,'RADIUS',7X,'B.O. TIME',7X,'TEMPERATURE',13X,'RATE',
       126X,'O2 FRACTION'//)
C     RGUES IS THE STARTING GUESS FOR THE COMBUSTION RATE
        RGUES=1.E-6
C     TGUES IS THE STARTING GUESS FOR PARTICLE TEMPERATURE.
        TGUES=TINF+300.
C     THE FOLLOWING LOOP IS USED TO DERIVE BURNOUT TIMES,TEMPERATURES
C     AND RATES FROM KEITH'S MODEL.
        DO 50 I=1,15
        Z=I-1
        RP(I)=0.66667*(RPO-RPO*Z/15.)

        CALL KEITH(TEMP,RAT,RP(I),TW,TGUES,TINF,PRESS,RGUES,FINO2)
        TIME(I)=.29452*RP(I)*RP(I)*RP(I)/RAT
        REALR(I)=1.50*RP(I)
        CALL KEITH(TE,PZ,REALR(I),TW,TGUES,TINF,XO2,RGUES,FINO2)
        TEMP=TE
        TP(I)=TE
        RATE(I)=PZ
        RAT=PZ
        TP(I)=TEMP
        RATE(I)=RAT
        WRITE(3,20)REALR(I),TIME(I),TP(I),RATE(I),FINO2
20      FORMAT(7X,2(F10.8,5X),F10.0,10X,E15.6,20X,F10.5)
50      CONTINUE
        WRITE(3,60)
60      FORMAT(////1X,'DMSLSS B.O. TIME',6X,'TEMPERATURE',10X,'REAL TIME',
       112X,'RADIUS'//)
C     THIS FOLLOWING LOOP IS USED TO GENERATE TEMPERATURE AS A FUNCTION
C     OF DIMENSIONLESS(AND REAL) BURNOUT TIMES.  RLTIM IS THE REAL
C     TIME AND DLST IS THE DIMENSIONLESS B.O. TIME.
```

```
      DO 80 J=1,15
      RLTIM(J)=TIME(1)-TIME(J)
      DLST(J)=RLTIM(J)/TIME(1)
      RMIC=10000.*REALR(J)
      WRITE(3,30)DLST(J),TP(J),RLTIM(J),RMIC
30    FORMAT(1X,F10.6,10X,F10.0,12X,F10.7,12X,F6.2)
80    CONTINUE
      SUM=0.
      DO 900 K=2,15
      DIFFT=DLST(K)-DLST(K-1)
      DIFFR=(RATE(K)+RATE(K-1))/2.
      SUM=SUM+DIFFT*DIFFR
900   CONTINUE
C     AVRAT IS THE TIME-AVERAGE OF THE RATE.  ONE CAN SEE IN THE
C     OUTPUT THAT IT IS EQUIVALENT TO THE RATE WHEN THE RADIUS IS
C     TWO-THIRDS ITS INITIAL VALUE.
      AVRAT=SUM/DLST(15)
      WRITE(3,910)AVRAT
910   FORMAT(///6X,'THE AVERAGE RATE OBTAINED BY NUMERICAL INTEGRATION =
     1',E15.6)
      CALL PUTPT(0,0,0.0,3000.,1.0,5500.,IJK,DLST,TP,15)
      CALL PDRAW(0,0,0.0,3000.,1.0,5500.,DLST,TP,15)
      IJK=IJK+1
      GO TO 1
      END
```

```
C   THIS PROGRAM WAS DESIGNED TO CRUNCH RAW DATA AND PRODUCE TEMPERATURE
C   PROFILES.  TWO INTENSITIES FROM TWO DIFFERENT WAVELENGTHS ARE FED
C   INTO THE PROGRAM ALONG WITH TIMES (INTO BURNOUT) AT WHICH THEY
C   WERE MEASURED.  THE TOTAL BURNOUT TIME IS ALSO FED.  GIVEN THE
C   CALIBRATION CONSTANT FROM A SEPARATE PROGRAM, THIS PROGRAM WILL
C   COMPUTE TEMPERATURES, DIMENSIONLESS BURNOUT TIMES AND AVERAGE
C   BURNOUT TIMES (ALONG WITH THE STANDARD DEVIATION)
C
      REAL LAMDA,LAMDB
      DIMENSION A(50),B(50),TIME(50),PHI(50),T(50)
      DIMENSION XTITL(5),YTITL(5)
      DATA YTITL/'TEMP','ERAT','URE ','(K) ','    '/
      DATA XTITL/'DIME','NSIO','NLES','S TI','ME  '/
      CALL LINSQ(3,0,0.0,1500.,1.0,5000.,XTITL,YTITL)
C   HERE I DEFINE THE WAVELENGTHS THAT ARE USED.  LAMDA CORRESPONDS
C   TO 'A' AND LAMDB TO 'B'.  IT IS IMPORTANT TO REMEMBER THAT THE
C   BANDWIDTHS MUST BE VERY NARROW IN ORDER TO USE THIS APPROACH.
C   OTHERWISE, ONE MUST INTEGRATE THE INTENSITY/WAVELENGTH CURVE.
      LAMDA=4.50E-5
      LAMDB=5.50E-5
      C2=1.44
      SUM=0.
      SUMSQ=0.
      WRITE(3,5)
 5    FORMAT('1COAL TYPE '/' COAL SIZE '/' GAS '/' GAS TEMPERATURE '/' W
     1AVELENGTHS '////)
      WRITE(3,7)
 7    FORMAT(' TEMP.    FRAC. BO. TIME        TIME   INTENS.A  INTENS.B'
     1)
C   'M' IS THE NUMBER OF PARTICLES WHOSE PROFILES ARE BEING DETERMINED.
C   THE CONSTANT IS PROVIDED BY ANOTHER PROGRAM
      READ(2,15)M,CONST
 15   FORMAT(I10,F10.5)
      DO 40 I=1,M
      READ(2,15)N,BOTIM
C   'N' IS THE NUMBER OF DATA POINTS TAKEN FOR ANY ONE PARTICLE.
C   BOTIM IS THE TOTAL APPARENT BURNOUT TIME.
      WRITE(3,17)I
 17   FORMAT(///' NEW PARTICLE  =',I10/)
      DO 20 J=1,N
C     EVERYTHING IS BEING PUT INTO ARRAYS SINCE I PLAN TO PLOT POINTS.
      READ(2,30)A(J),B(J),TIME(J)
 30   FORMAT(3F10.6)
      T(J)=C2*(1./LAMDB-1./LAMDA)/(ALOG(A(J)/B(J))-CONST)
      PHI(J)=TIME(J)/BOTIM
      WRITE(3,50)T(J),PHI(J),TIME(J),A(J),B(J)
 50   FORMAT(F10.0,F10.4,5X,3F10.5)
 20   CONTINUE
C   THE PLOTTING ROUTINES ARE USED TO GRAPH TEMPERATURE VS.
C   DIMENSIONLESS TIME.
      CALL PDRAW(0,0.0,0.0,1500.,1.0,5000.,PHI,T,N)
      SUM=SUM+BOTIM
      SUMSQ=SUMSQ+BOTIM**2.
      IF(I.EQ.M)GO TO 60
 40   CONTINUE
 60   AA=M
C     THESE FOLLOWING 3 LINES CALCULATE THE AVERAGE BURNOUT TIME AS WELL
C     AS THE STANDARD DEVIATION.
      VAR=(SUMSQ-SUM**2./AA)/(AA-1.)
      STDEV=SQRT(VAR)
      AVGBO=SUM/AA
      WRITE(3,70)AVGBO,STDEV
 70   FORMAT(///' AVERAGE BURNOUT TIME = ',E20.5/'    STANDARD DEVIATION
     1 =',E20.5)
      CALL PSKIP
      STOP
      END
```

APPENDIX D - RAW DATA

The following pages show (computer) plots of all the temperature data from series E, F, G, J and K. The B series is omitted because of the higher uncertainties associated with its calibrations. Average values for this series are in Table 5.2.

All of the temperature profiles were created by making straight line connections between consecutive data points. This is somewhat deceiving and not highly accurate, but it gives the reader an idea of the variations that exist within a single burnout and between different particles. The data seen in these next few pages have been averaged, and the results are presented in the text in Table 5.2.

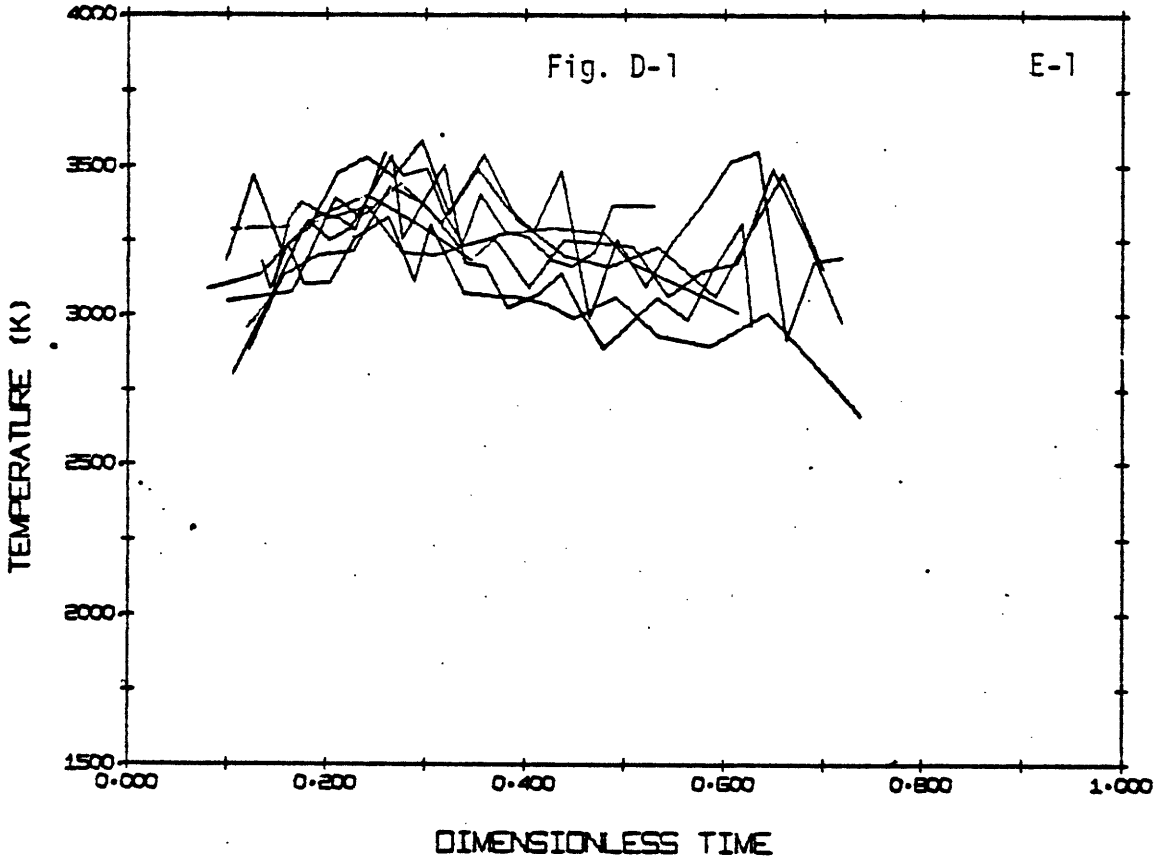
Fig. D-1
E-1
TEMPERATURE (K)
4000
3500
3000
2500
2000
1500
0.000
0.200
0.400
0.600
0.800
1.000
DIMENSIONLESS TIME

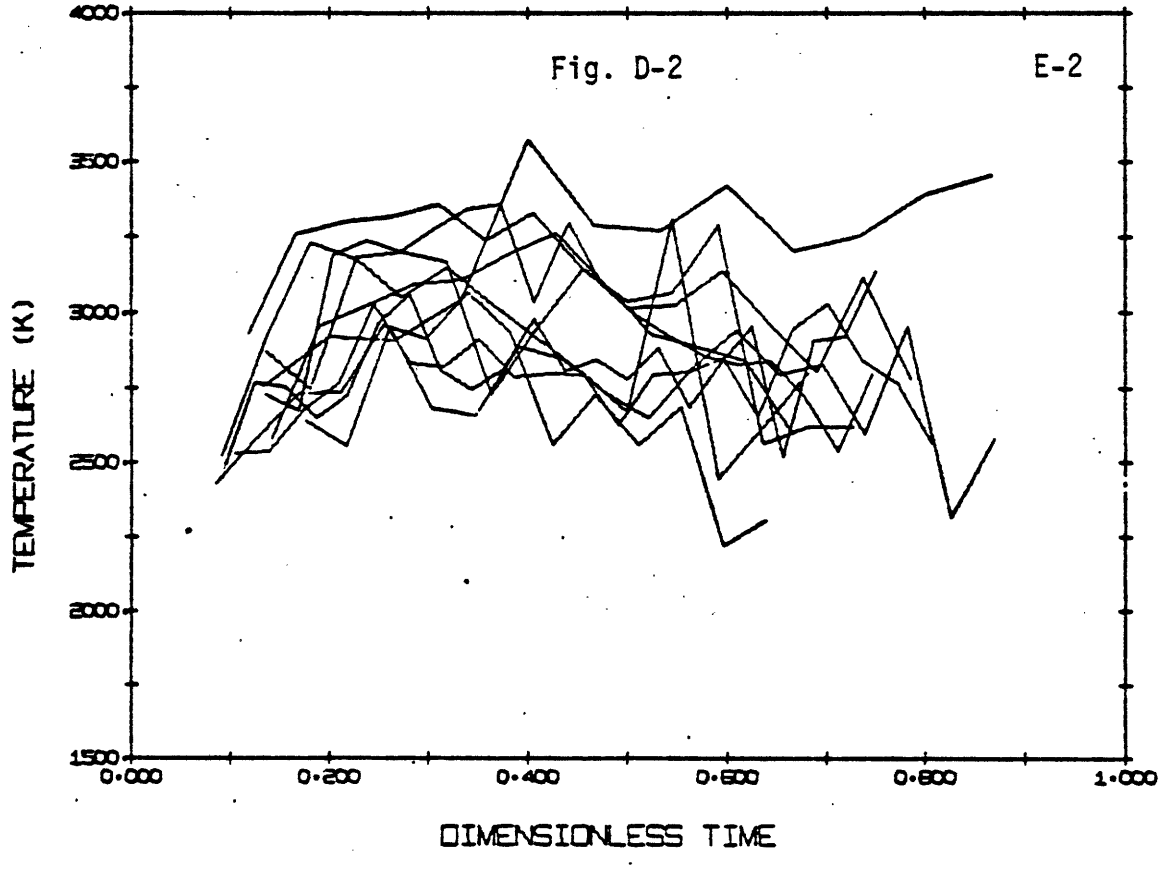
Fig. D-2
E-2
TEMPERATURE (K)
4000
3500
3000
2500
2000
1500
0.000
0.200
0.400
0.600
0.800
1.000
DIMENSIONLESS TIME

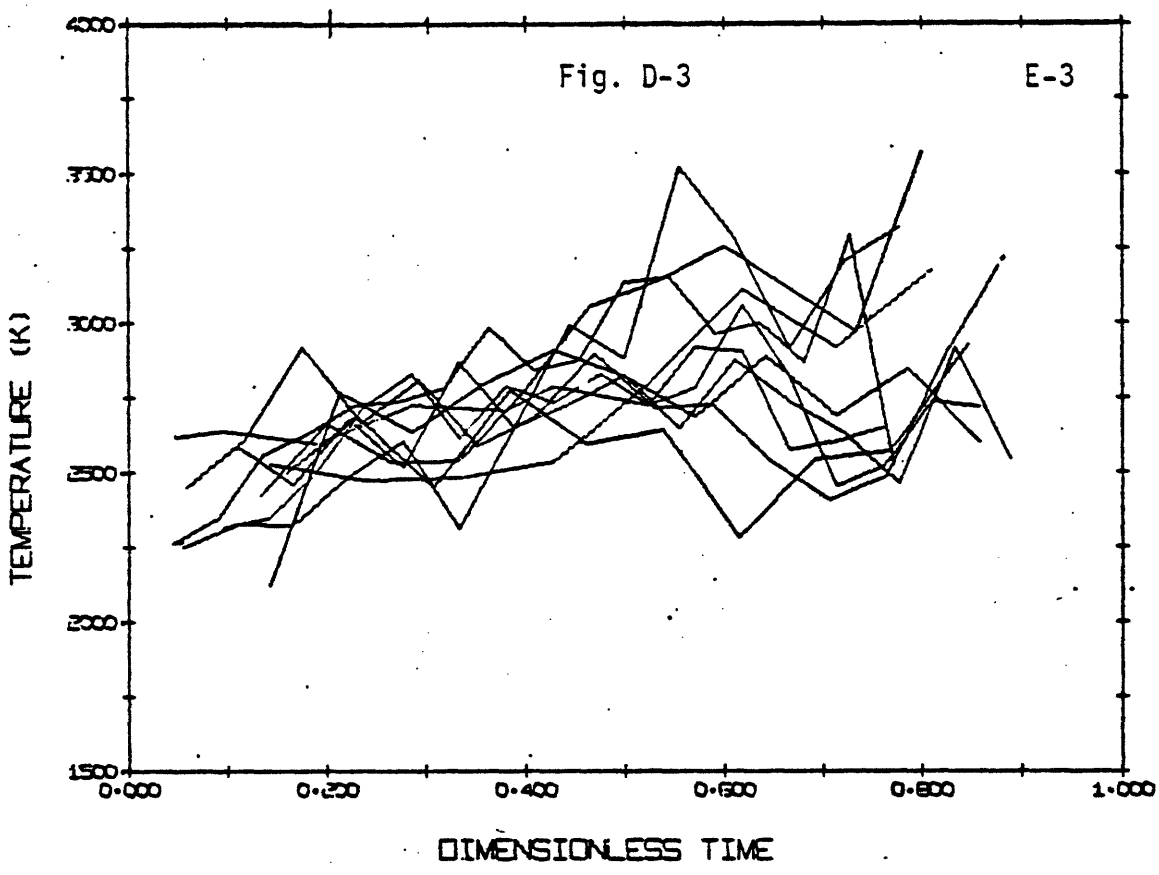
Fig. D-3
E-3
TEMPERATURE (K)
4000
3500
3000
2500
2000
1500
0.000
0.200
0.400
0.600
0.800
1.000
DIMENSIONLESS TIME

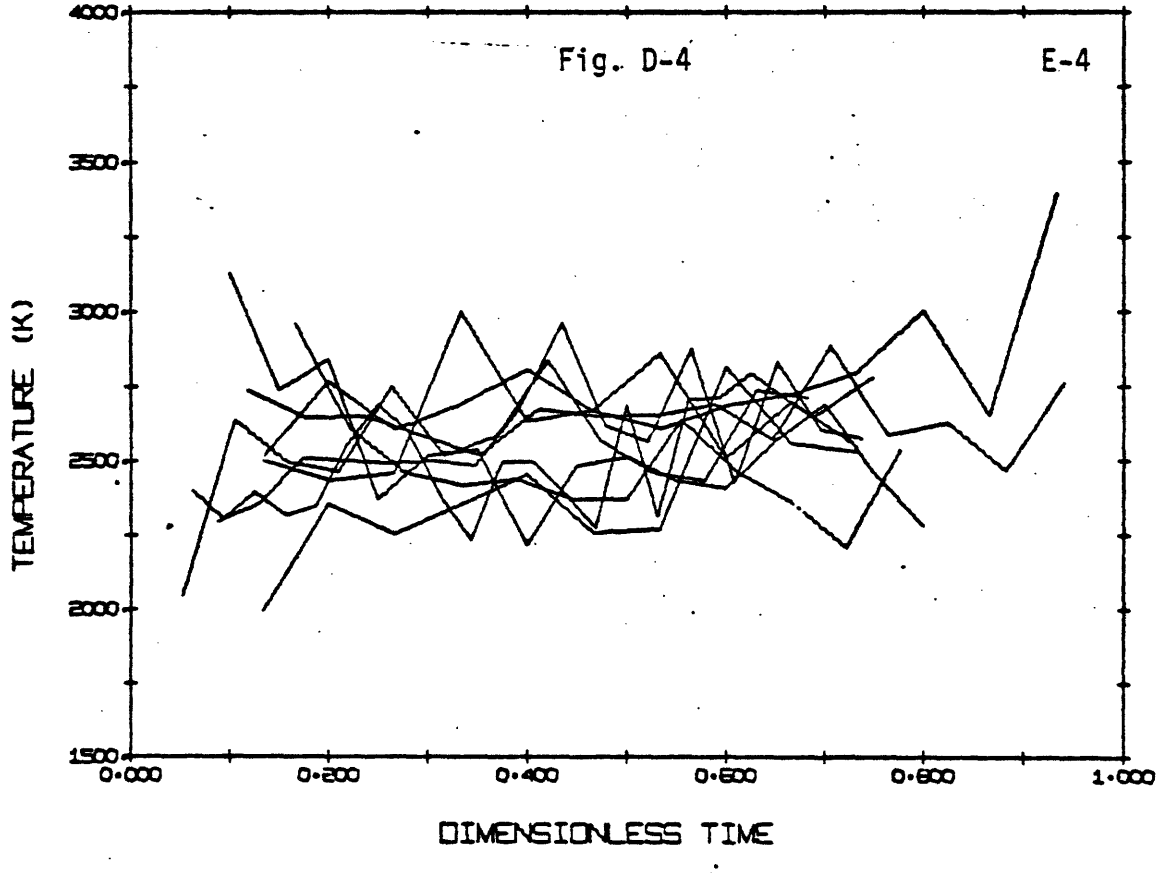
Fig. D-4
E-4
TEMPERATURE (K)
4000
3500
3000
2500
2000
1500
0.000
0.200
0.400
0.600
0.800
1.000
DIMENSIONLESS TIME

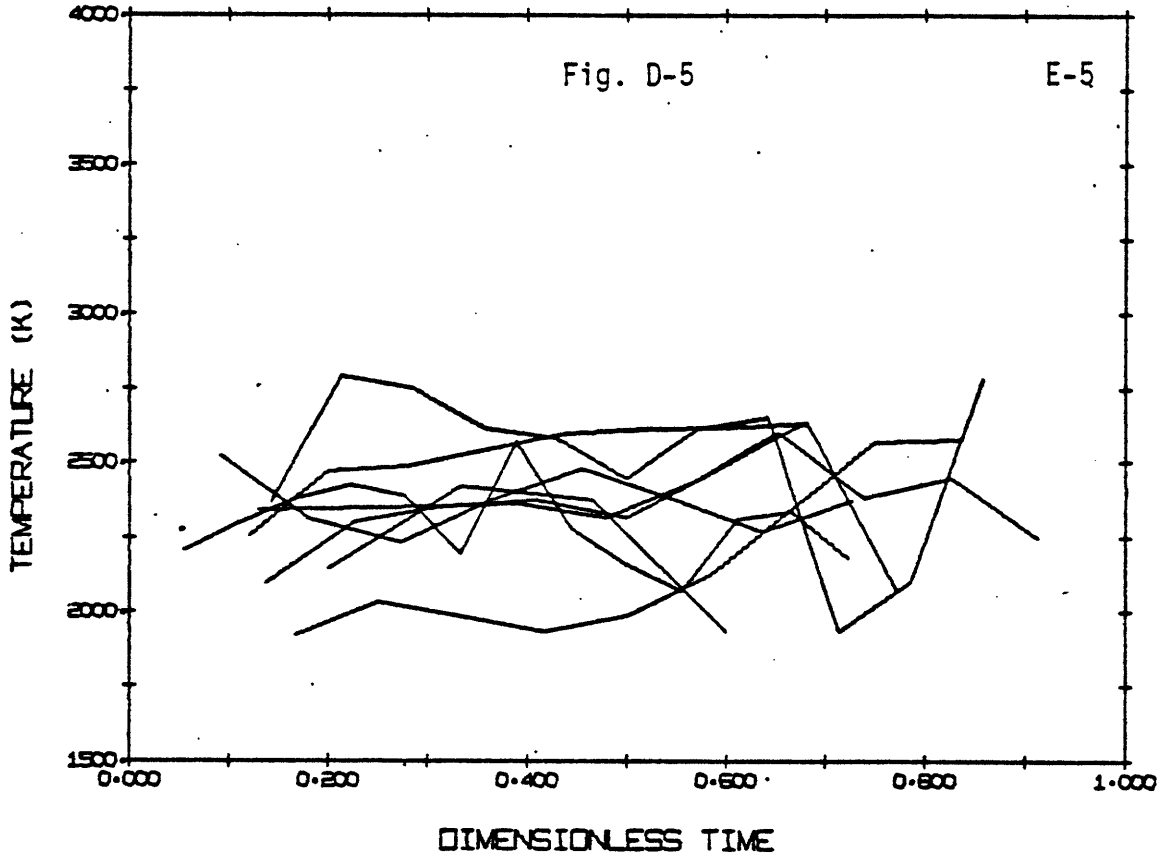
Fig. D-5
E-5
4000
3500
3000
2500
2000
1500
TEMPERATURE (K)
0·000
0·200
0·400
0·600
0·800
1·000
DIMENSIONLESS TIME

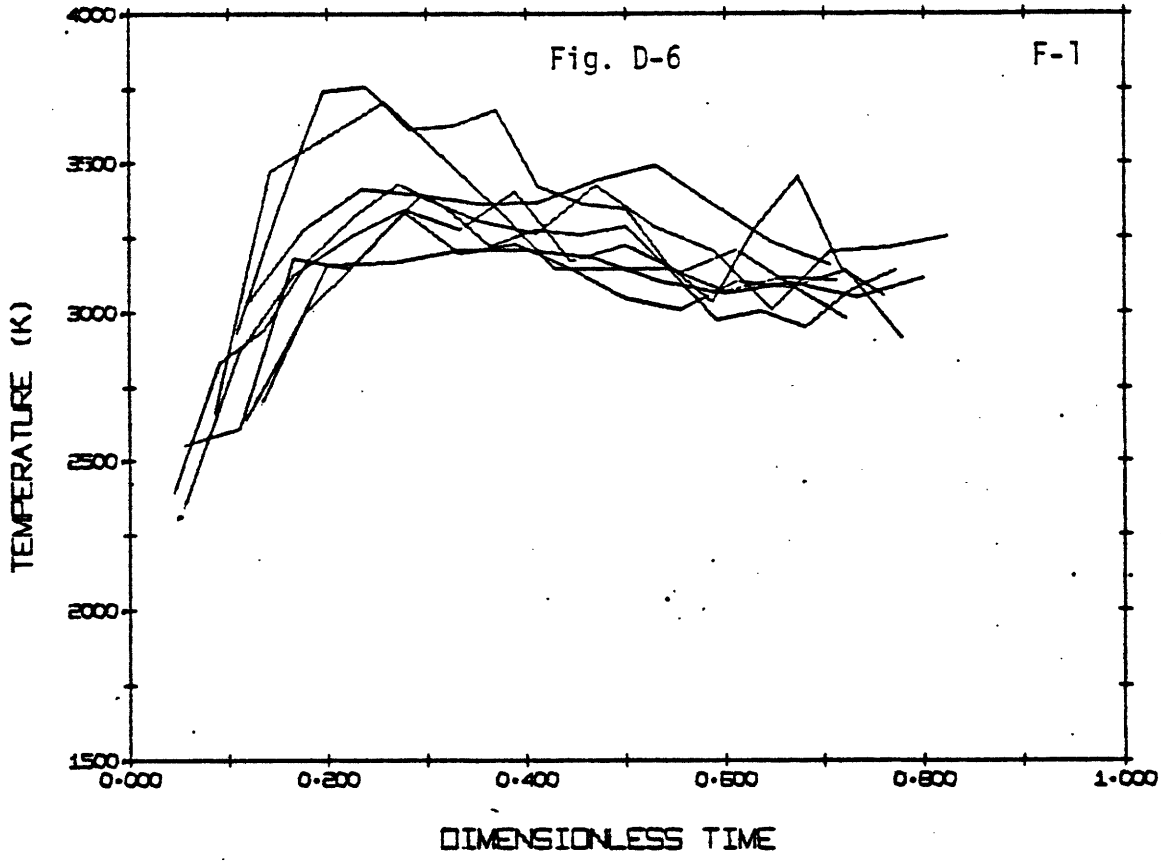
Fig. D-6
F-1
TEMPERATURE (K)
4000
3500
3000
2500
2000
1500
0.000
0.200
0.400
0.600
0.800
1.000
DIMENSIONLESS TIME

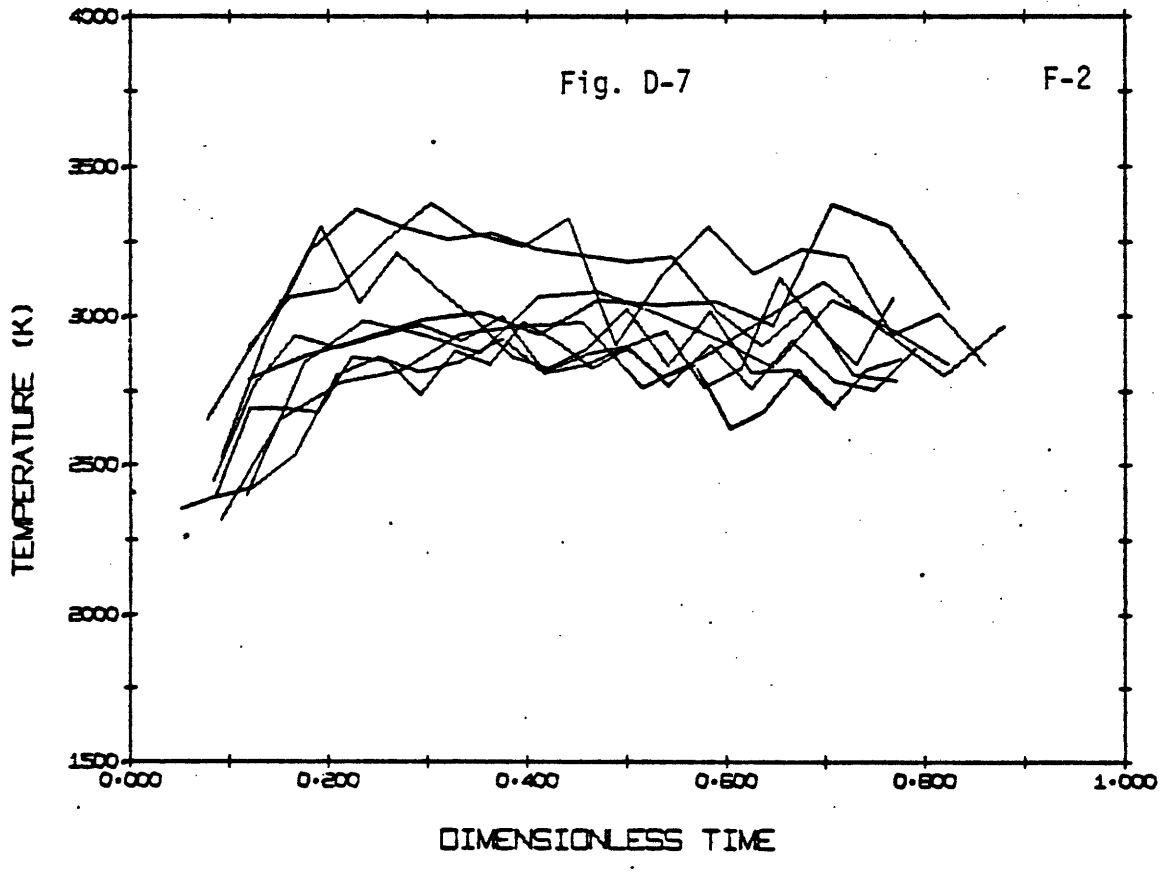
Fig. D-7
F-2
TEMPERATURE (K)
4000
3500
3000
2500
2000
1500
0.000
0.200
0.400
0.600
0.800
1.000
DIMENSIONLESS TIME

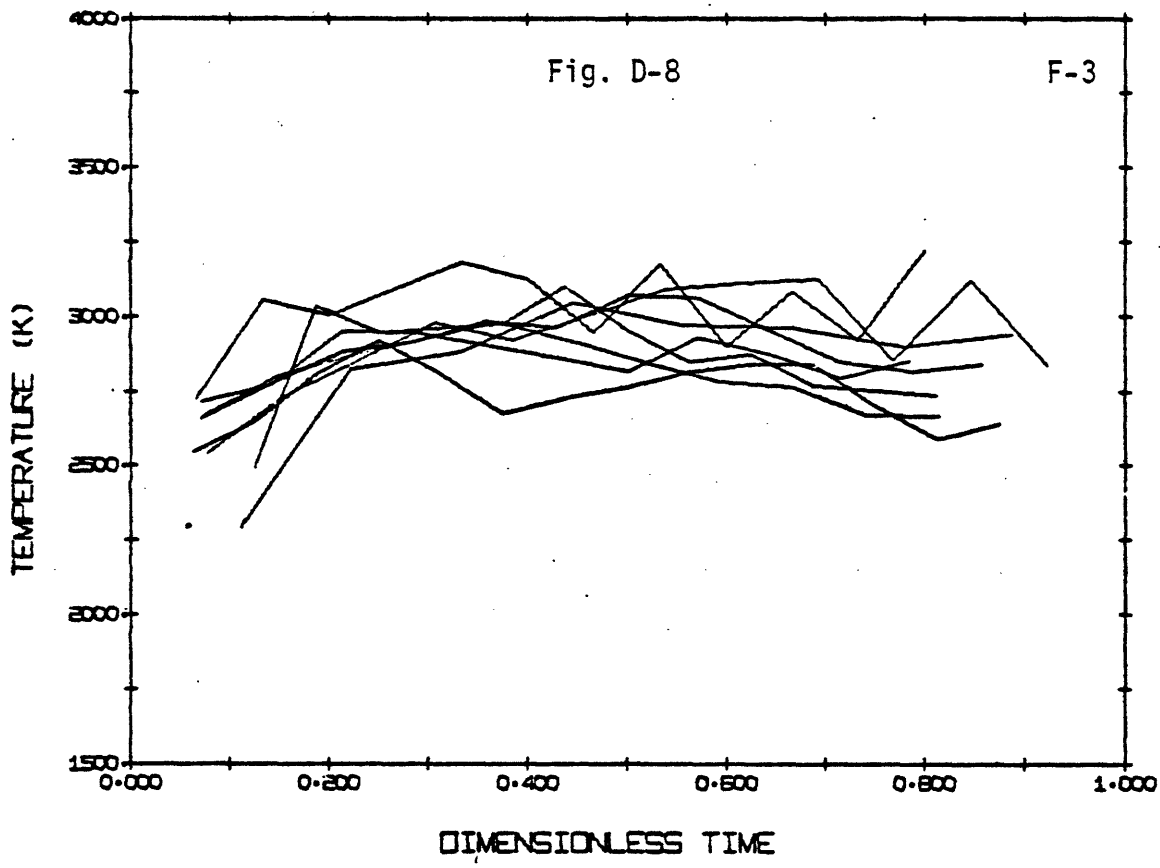
Fig. D-8
F-3
TEMPERATURE (K)
4000
3500
3000
2500
2000
1500
0.000
0.200
0.400
0.600
0.800
1.000
DIMENSIONLESS TIME

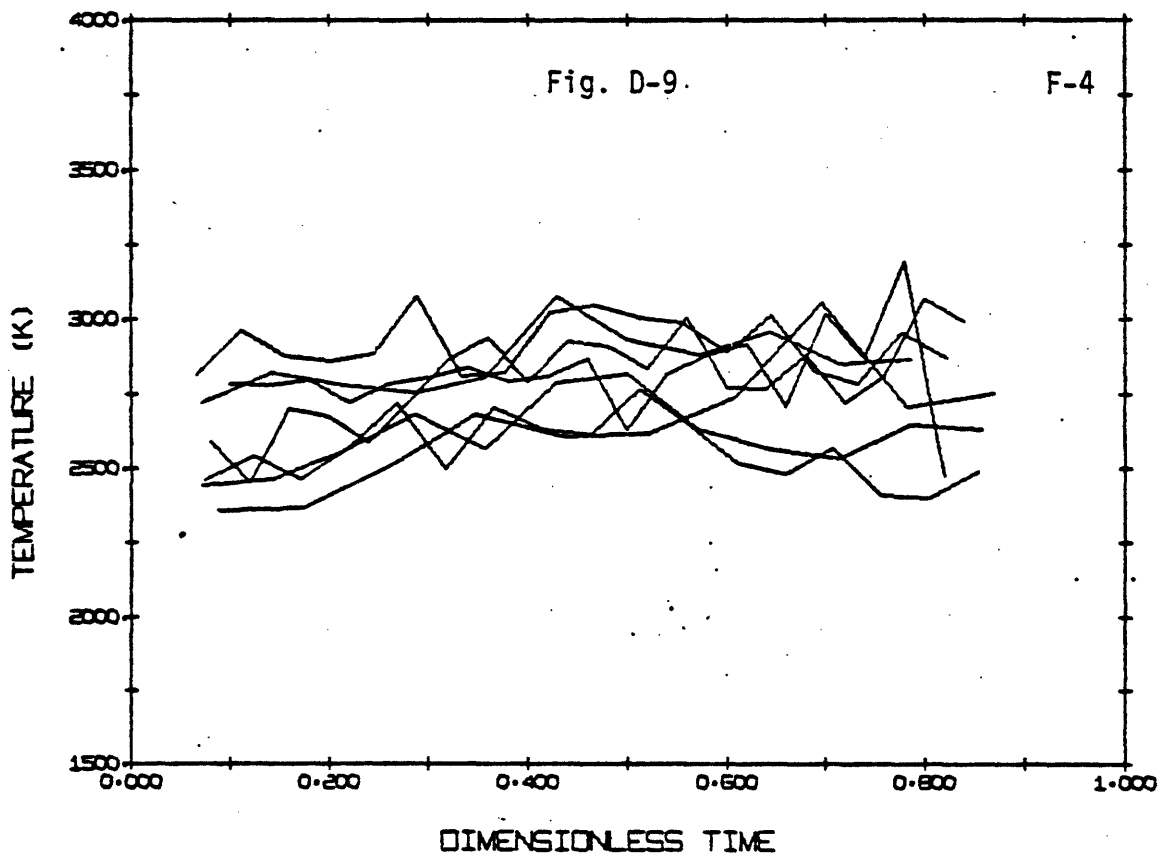
Fig. D-9
F-4
TEMPERATURE (K)
4000
3500
3000
2500
2000
1500
0.000
0.200
0.400
0.600
0.800
1.000
DIMENSIONLESS TIME

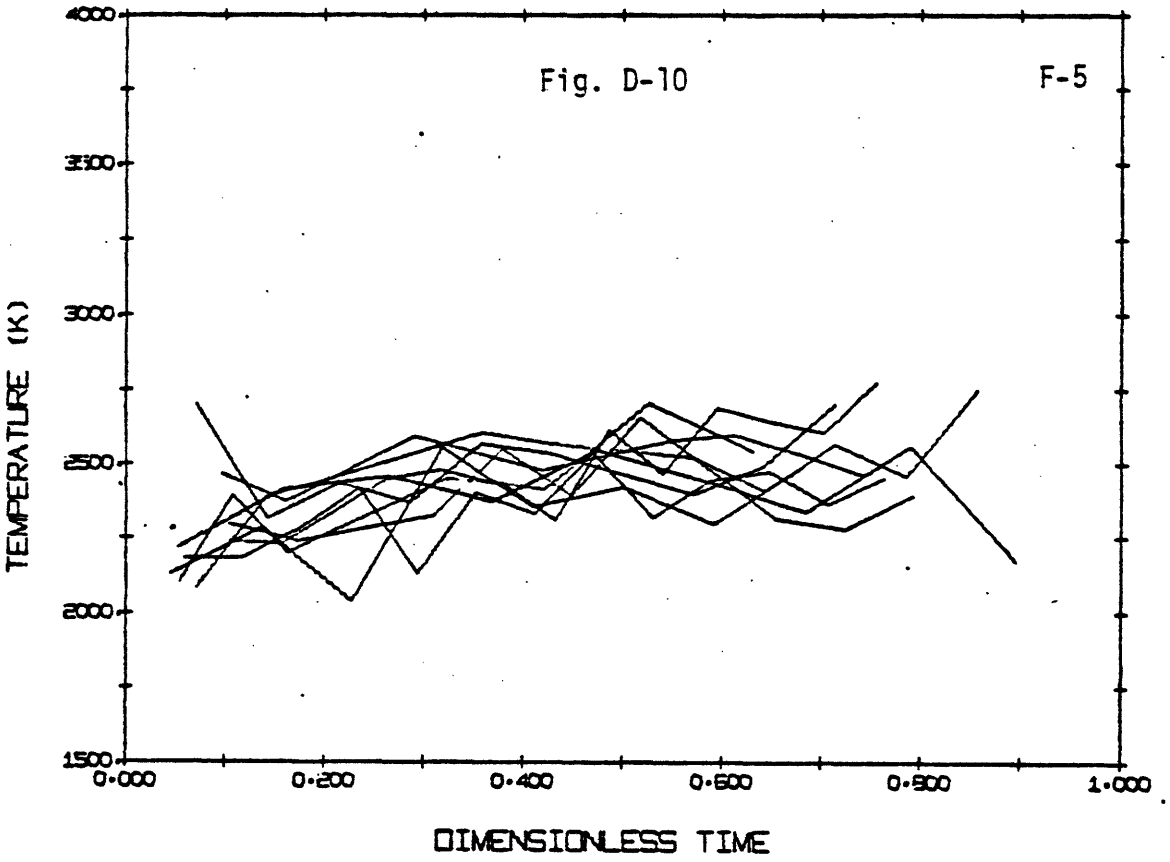
Fig. D-10
F-5
TEMPERATURE (K)
4000
3500
3000
2500
2000
1500
0.000
0.200
0.400
0.600
0.800
1.000
DIMENSIONLESS TIME

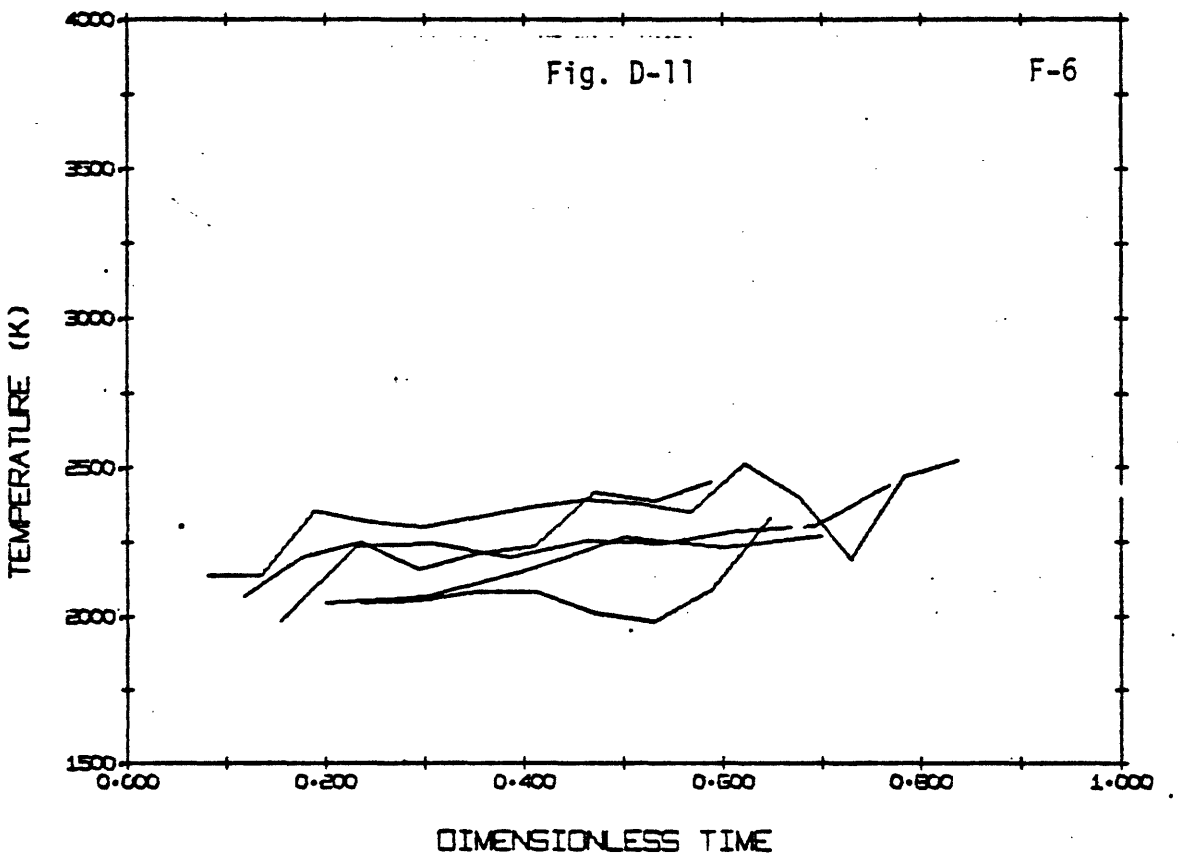
Fig. D-11
F-6
TEMPERATURE (K)
4000
3500
3000
2500
2000
1500
0.000
0.200
0.400
0.600
0.800
1.000
DIMENSIONLESS TIME

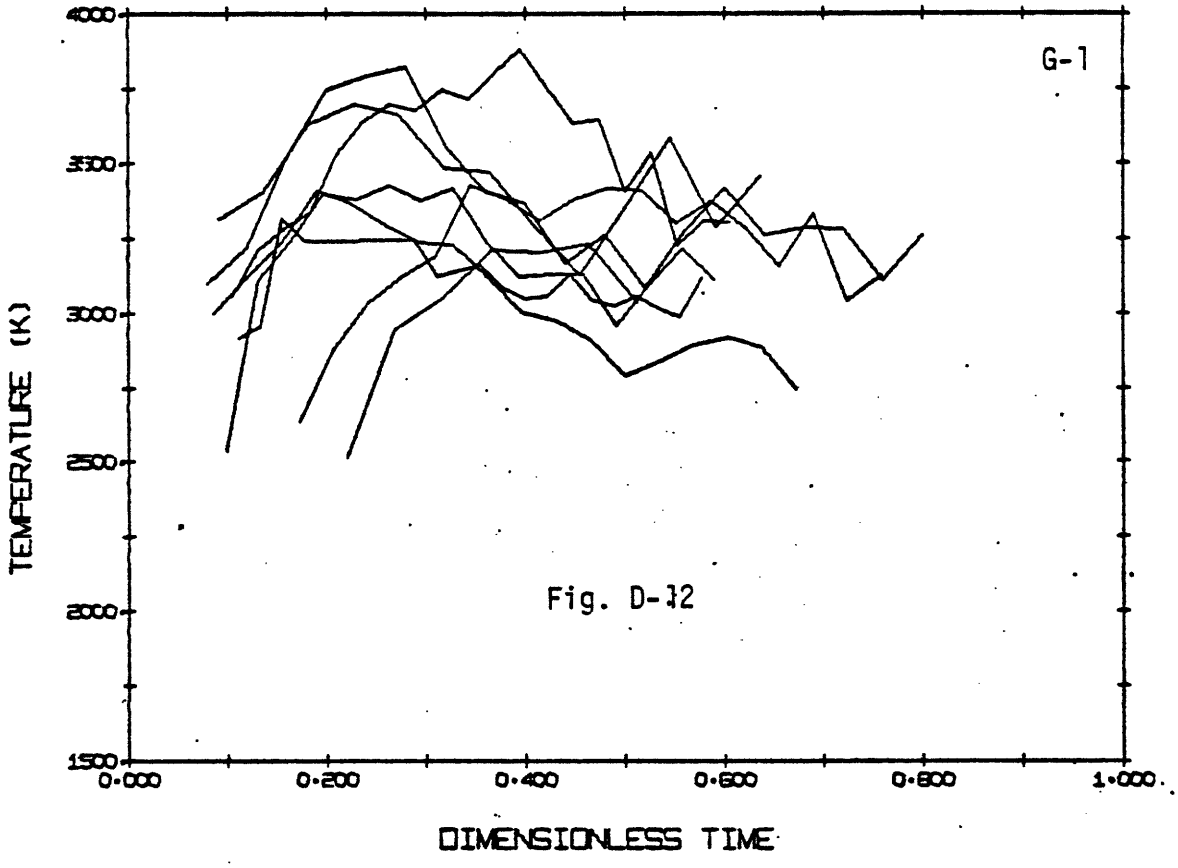

Fig. D-12

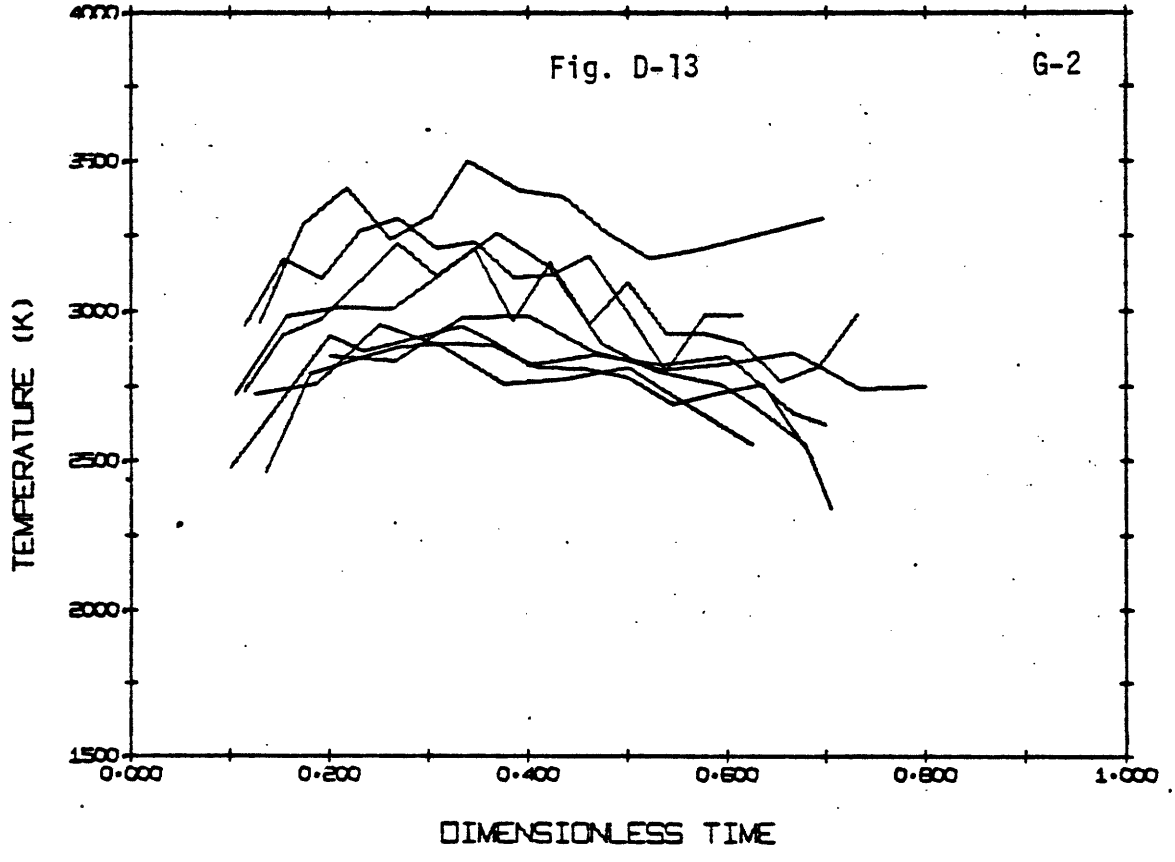

Fig. D-13

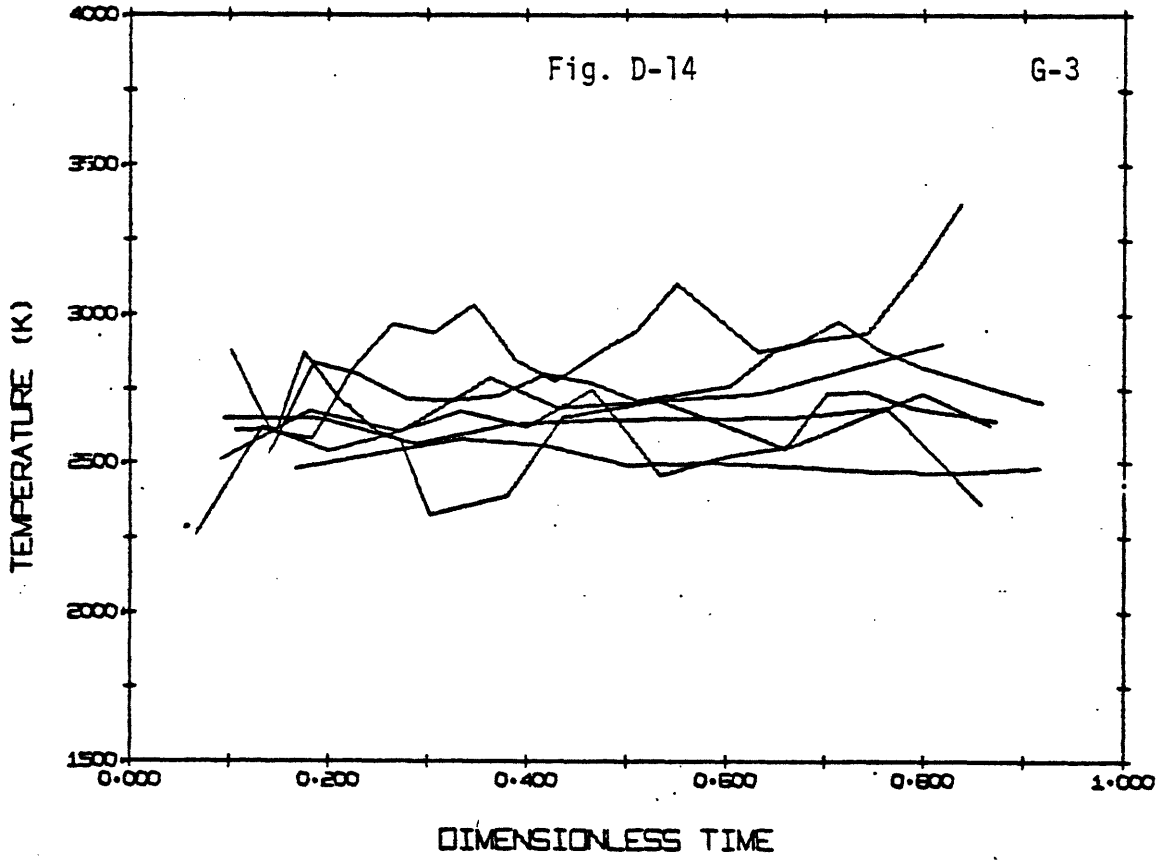
Fig. D-14
G-3
4000
3500
3000
2500
2000
1500
TEMPERATURE (K)
0.000
0.200
0.400
0.600
0.800
1.000
DIMENSIONLESS TIME

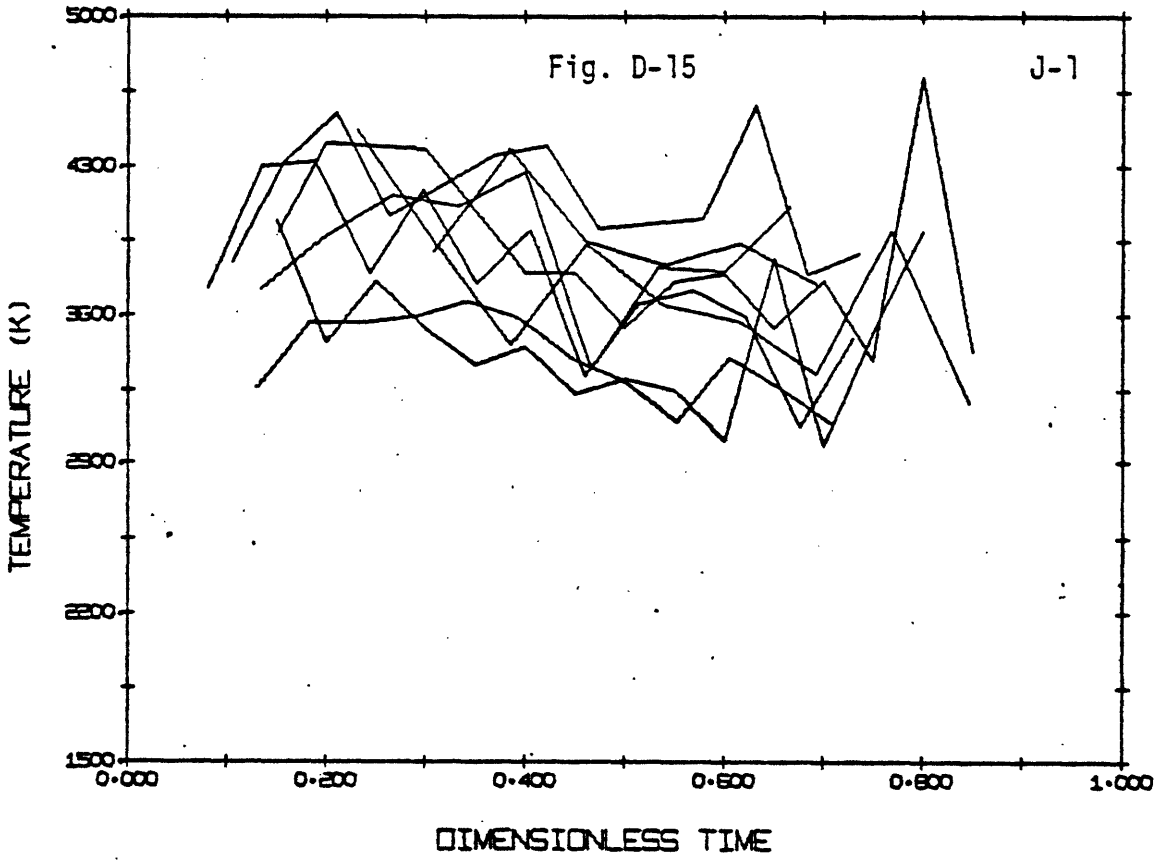
Fig. D-15
J-1
TEMPERATURE (K)
5000
4300
3600
2900
2200
1500
0.000
0.200
0.400
0.600
0.800
1.000
DIMENSIONLESS TIME

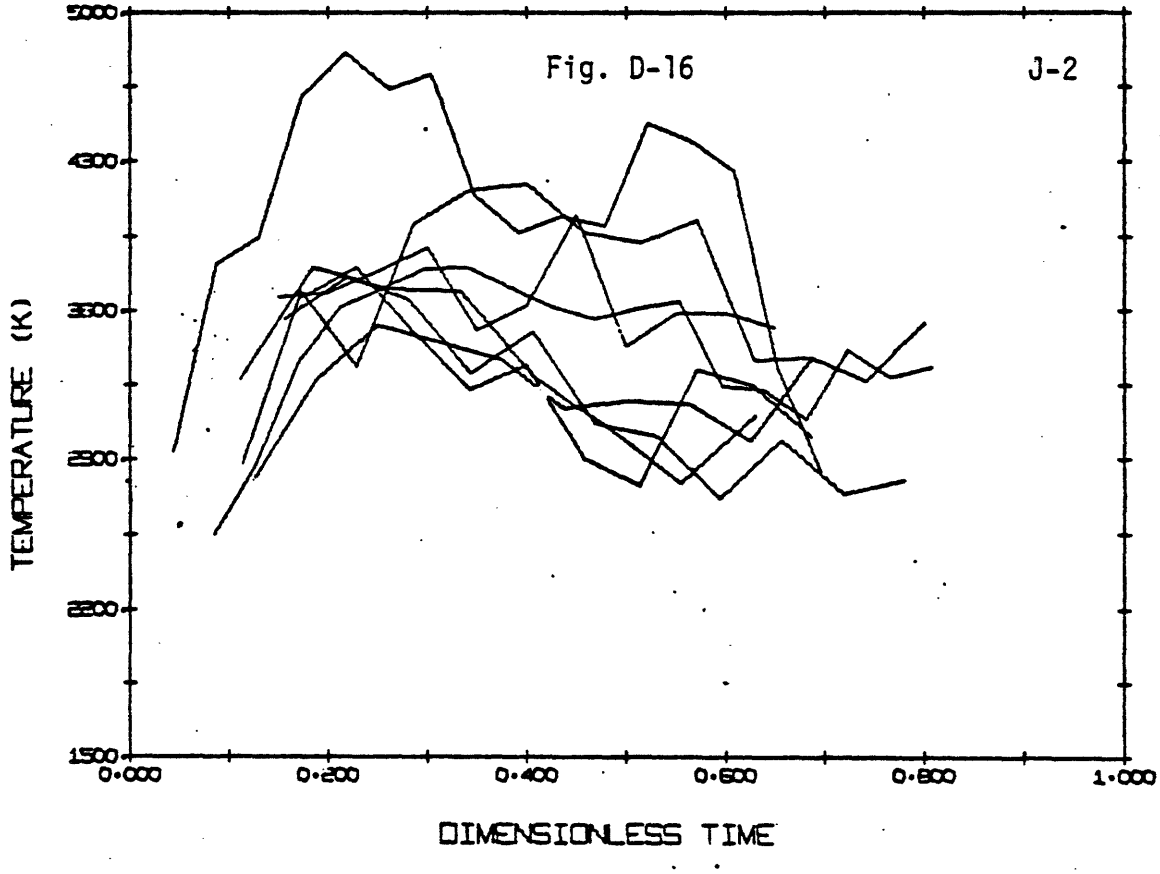
Fig. D-16
J-2
TEMPERATURE (K)
5000
4300
3600
2900
2200
1500
0.000
0.200
0.400
0.600
0.800
1.000
DIMENSIONLESS TIME

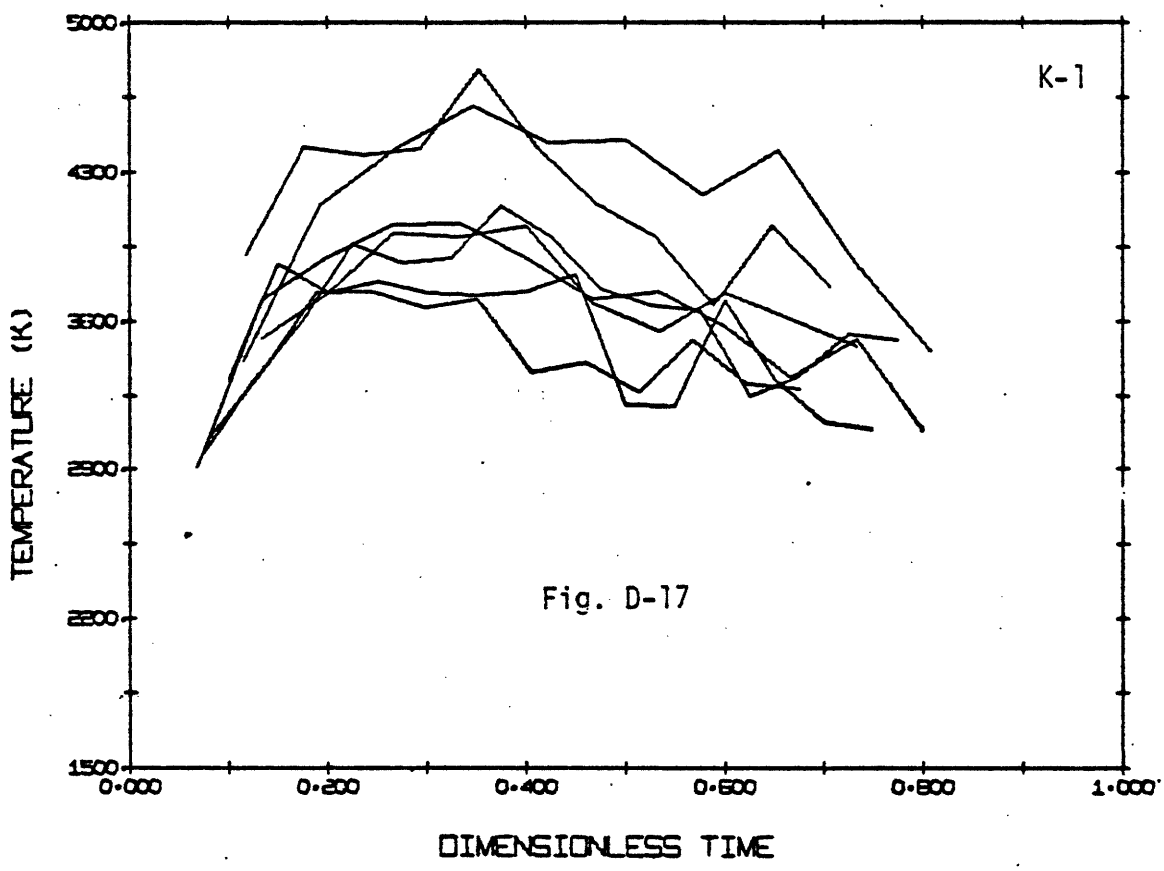

Fig. D-17

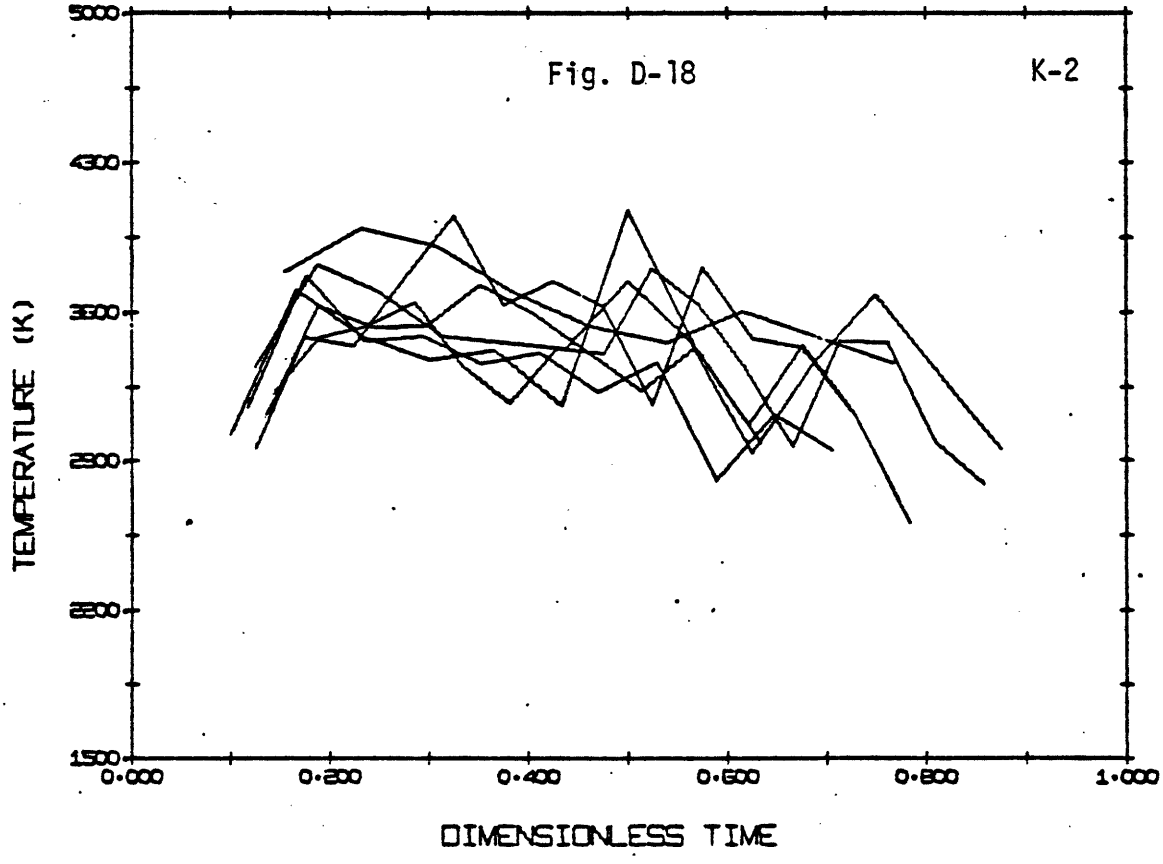

Fig. D-18

REFERENCES

1. Amundson, N.R. and H.S. Caram, "Diffusion & Reaction in a Stagnant Boundary Layer about a Carbon Particle," Ind. Eng. Chem. Fundam., Vol. 17 (1978), pp. 171-181.

2. Ayling, A.B. and I.W. Smith, "Measured Temperatures of Burning Pulverized Fuel Particles, and the Nature of the Primary Reaction Product," Combustion and Flame, Vol. 18, (1972), pp. 173-184.

3. Bird, R.B. et al., Transport Phenomena, John Wiley & Sons, Inc., New York (1960) p. 510.

4. Butler, J.N. and R.S. Brokaw, "Thermal Conductivity of Gas Mixtures in Chemical Equilibrium," J.Phys. Chem., Vol. 26, (1957) pp. 1636-1643.

5. DeVos, J.C., "A New Determination of the Emissivity of Tungsten Ribbon," Physica, Vol. 20, (1954) pp. 690-714.

6. Field, M.A. et al., Combustion of Pulverized Coal, BCURA, (1967) p. 175.

7. Hottel, H.C. and F.P. Broughton, "Determination of True Temperature and Total Radiation from Luminous Gas Flames," Ind. Eng. Chem., Vol. 4, (1932), pp. 166-174.

8. House, K., "Design and Testing of a Two Color Pyrometer for Application in Coal Particulate Temperature Measurement," B.S. Thesis, MIT Dept. of Chemical Engineering (1978).

9. JANAF Thermochemical Tables NSRDS-NBS (1971).

10. National Bureau of Standards Monograph 41: "Theory and Methods of Optical Pyrometry," (1962).

11. Rae, D., "A Measurement of the Temperature of Some Frictional Sparks," Combustion and Flame, Vol. 5, (1961) pp. 341-347.

12. Rutgers, G.A.W. and J.C. DeVos, "Relation Between Brightness Temperature, True Temperature and Colour Temperature of Tungsten. Luminance of Tungsten." Physica, Vol. 20 (1954), pp. 715-720.

13. Ubhayakar, S.K. and F.A. Williams, "Burning and Extinction of a Laser - Ignited Carbon Particle in Quiescent Mixtures of Oxygen and Nitrogen," J.Electrochem. Soc., Vol. 123, (1976) pp. 747-756.